

Research Paper

Fruit cooling performance analysis within a fully loaded refrigerated container: CFD modelling and validation



Tarl M. Berry ^{a,b,*}, Nurayn A. Tiamiyu ^{b,c}, Jacques van Zyl ^{a,c}, Umezuruuke L. Opara ^{b,d}, Paul Cronje ^a, Alemanyehu Ambaw ^b, Vaughan Hattingh ^a, Corné Coetzee ^c, Thijs Defraeye ^{e,f}

^a Citrus Research International, Department of Horticultural Sciences, Stellenbosch University, Stellenbosch, 7600, South Africa

^b Africa Institute for Postharvest Technology, Department of Horticultural Sciences, Faculty of AgriSciences, Stellenbosch University, Stellenbosch, 7600, South Africa

^c Department of Mechanical and Mechatronics Engineering, Stellenbosch University, Private Bag X1, Matieland 7600, South Africa

^d UNESCO International Centre for Biotechnology, Nsukka, 410001, Enugu State, Nigeria

^e Empa, Swiss Federal Laboratories for Materials Science and Technology, Laboratory for Biomimetic Membranes and Textiles, Lerchenfeldstrasse 5, CH-9014, St. Gallen, Switzerland

^f Food Quality and Design, Wageningen University & Research AA Wageningen, P.O. Box 17, 6700, the Netherlands

ARTICLE INFO

ABSTRACT

Keywords:

Citrus
Shipping
Cold chain
Fresh produce
Computational fluid dynamics
Packaging
Temperature monitoring

Refrigerated containers (RCs) are crucial for transporting fresh produce to international markets, significantly influencing fruit quality along the cold chain. Although RCs are a mature technology, fresh produce industries report challenges relating to temperature heterogeneity and ineffective monitoring approaches. This study developed and validated a computational fluid dynamics model to characterise airflow and heat transfer inside an RC packed with standard ventilated packaging for South African citrus fruit. The model was implemented with an accurate representation of a refrigeration unit, incorporating the presence of fans and evaporator coils based on experimental characterisations. Air speed and cooling validations showed good agreement with the models. Simulations identified a vertically dominant airflow pattern, with air speeds within the pallets ranging from 0.03 m s^{-1} to 0.16 m s^{-1} . Air velocities within the pallet regions were categorised into four zones: a turbulent air recirculation zone, a high-velocity stabilisation zone, a declining air velocity zone, and a heterogeneous air velocity zone near the door. Excessively cooled regions were identified, potentially increasing chilling injury risk, a primary concern for South African citrus exports. The study evaluated temperature monitoring, and an optimal position for hygrothermal sensors was proposed for single-device monitoring. It was further shown that air temperature data is conditionally representative of pulp temperature. The insights gained can guide industry practitioners in enhancing temperature monitoring practices and inform future research on optimising RC cooling efficiency and minimising chilling injury risks to improve fruit quality and reduce waste in the fresh produce supply chain.

Nomenclature

(continued)

Abbreviations

| | |
|---------------------|---|
| CFD | Computational fluid dynamics |
| LTE | Local thermal equilibrium |
| LTNE | Local thermal non-equilibrium |
| RC | Refrigerated Container |
| RSD | Relative standard deviation percentage (%) |
| RU | Refrigeration unit |
| sMAPE | Symmetric mean absolute percentage error |
| SST $\kappa-\omega$ | Shear-Stress-Transport $\kappa-\omega$ turbulence model |
| TFCT | Three-Fourths cooling time |

(continued on next column)

Symbols

| | |
|-------|--|
| d | characteristic length (diameter), m |
| P | Pressure, Pa |
| Q | Flow rate ($\text{m}^3 \text{ s}^{-1}$) |
| R^2 | Coefficient of determination |
| Re | Reynolds number |
| t | Time, s |
| T | Temperature, K ($^\circ\text{C}$ in analysis) |
| u | Air velocity, m s^{-1} |

(continued on next page)

* Corresponding author. Citrus Research International, Department of Horticultural Sciences, Stellenbosch University, Stellenbosch, 7600, South Africa.
E-mail address: tarl@sun.ac.za (T.M. Berry).

(continued)

| | |
|---------------------|---|
| Y | Dimensionless temperature (Supplementary materials: Section S1.5) |
| Greek symbol | |
| ΔT | Difference between air and pulp (K) |
| ΔP | Pressure drop (Pa) |
| ρ | Density, kg m ⁻³ |
| ϕ | Recommended probe position |
| μ | Dynamic viscosity, kg m ⁻¹ s ⁻¹ |
| ω | Directional airflow resistance coefficient, kg m ⁻⁴ |
| Subscript | |
| a | Air |
| eq | Stabilisation time |
| i | Initial temperature |
| p | Pulp |

1. Introduction

Refrigerated transport is an essential component of the horticultural cold chain system, which also includes pre-cooling of fruit, cold storage, and refrigerated displays at retail outlets (Berry, Shrivastava, et al., 2022; Thompson et al., 2010). Fresh produce temperature is an essential factor that affects fruit senescence rates, quality preservation, and shelf life (Robertson, 2013; Thompson et al., 2010). In addition, low temperatures are applied in some industries to eradicate live pests within the produce (Moore et al., 2016; Moore & Hattingh, 2016). During the past four decades (>1980), the integrated refrigerated container (RC) has become the preferred mode for transporting fresh produce over long distances. South Africa ships out approximately 100,000 citrus containers a year to markets worldwide. The international export of fresh produce using RCs is a relatively mature industry; however, the complex cooling environment has resulted in little optimisation of RC usage to more effectively and efficiently transport fresh produce (Maiorino et al., 2021; Wild, 2014). There is still insufficient knowledge of the airflow, associated fruit cooling process and cooling heterogeneity of the fruit within the ventilated cargo for the multitude of fresh produce species and packaging designs (Lukasse et al., 2023).

The cooling processes during RC shipping of citrus fruit considerably impact quality preservation and chilling injury, which significantly impacts market sustainability and food waste (Cronje et al., 2011). Losses due to chilling injury constitute a significant issue for citrus fruit in South Africa (Zacarias et al., 2020), and other tropical products globally (Heyes, 2023). Container set points are typically set so that the warmest regions meet quality or phytosanitary requirements. However, the temperature heterogeneity within the container can result in hyper-cold regions that significantly increase the probability of chilling injury. Prior works have also noted the potential presence of a recirculation airflow region in the lower regions of the pallets adjacent to the refrigeration unit (Defraeye et al., 2022, 2024; Getahun et al., 2017a; Senguttuvan et al., 2021).

Temperature monitoring of loaded RCs can often be a challenge to both commercial operations and academic studies. From an academic perspective, validation experiments benefit significantly from higher resolutions of temperature monitoring. One standard solution is to simplify the experimental validation, and many studies have thus made use of a partially loaded or scaled RC (Defraeye et al., 2024; Jedermann et al., 2013; Moureh et al., 2002; Senguttuvan et al., 2020, 2021). Commercially, industry role players must monitor container cooling throughout the supply chain. Several million containers are shipped yearly to global markets (Food and Agriculture Organization FAO, 2021), and the complex logistical handling of these cargoes can result in extended transit delays and cold chain breaks, which can significantly impact quality preservation. Oversight of the cold chain is thus key to optimising the overall supply chain. Enhanced monitoring and, more

importantly, interpretation of temperature data can significantly contribute to mitigating supply chain risks and minimising food wastage.

Traditionally, fruit pulp temperatures have been the preferred monitoring mode, as they directly represent the thermal environment influencing fruit metabolism (Thompson et al., 2008). However, as a cost-saving measure, most commercial exporters only utilise air temperature loggers to monitor conditions during shipping, and a review of the literature shows no studies or guidelines for how air temperature loggers should be interpreted or installed in RC during shipping.

From a commercial perspective, the cost of temperature loggers and the practicality of placement thereof makes it economically impractical to monitor RCs temperature at high resolutions by installing multiple temperature loggers throughout the container. There is no published literature detailing the optimal probing location in an RC, although some recommendations are available from in-transit cold treatment documents (phytosanitary). Specifically, Food and Agriculture Organization FAO, (2018) proposes a container probe location “that will take the longest time to reach the required core temperature”. The recommendation is purposefully vague to accommodate a plethora of different product types and shipping modes. The geometrical setup of the pallet load-out and the packaging type (airflow resistance) will significantly impact the cooling patterns. The respective monitoring position should thus be specific to the respective setup. However, even a general monitoring strategy for commercial operations is still lacking.

The control of air temperature and the circulation of air inside a RC depends on several factors, which include: (i) the refrigeration unit type and model; (ii) the operational software protocol of the refrigeration unit for the temperature and the fan operation, for example Maersk's QUEST II system (Lukasse et al., 2011); (iii) the precooling of the fruit, i.e. the remaining field heat in the fruit; (iv) the container's thermal insulation (Laguerre et al., 2008); (v) flooring design (Smale, 2004; Wild, 2014); (vi) pallet stacking patterns; (vii) packaging designs (Berry et al., 2016; Defraeye et al., 2013; Fadiji et al., 2016; Getahun et al., 2017a; Getahun et al., 2017b; O'Sullivan et al., 2017; Tanner & Amos, 2003); and (viii) container loading aids/modifications (Defraeye et al., 2016; Jiang et al., 2020). Exploring these factors experimentally across multiple treatments and repeats at these scales is prohibitively impractical due to the enormous costs, food losses and large quantities of measurement equipment needed to evaluate fully loaded containers. Numerical physics-based simulations are often a more suitable alternative tool to explore the RC design space conceptually.

In recent years, computational fluid dynamics (CFD) has emerged as the most widely used predictive tool for investigating airflow distribution and temperature evolution in cold chain applications, offering relatively accurate predictions with moderate computational demands (Mukama et al., 2020; Norton & Sun, 2006; Verboven et al., 2006). CFD solves the Navier-Stokes equations for the conservation of mass and momentum in the respective geometry and heat conduction inside the fruit. However, explicit modelling of very large-scale systems, such as RCs packed with tens of thousands of individual fruits, is currently computationally prohibitive due to the high resolution required to represent each fruit and its packaging (Ajani et al., 2021).

A porous media approach is commonly employed to address this problem by simplifying the packed produce into a continuous medium with averaged properties like porosity and permeability. This can reduce computational complexity by one or two orders of magnitude while still capturing the essential heat and airflow dynamics using modified equations for conservation laws. Although detailed CFD modelling offers greater accuracy, its feasibility is often not viable in large systems, making the porous media approach a practical and widely accepted alternative (Zhao et al., 2016). Even then, the previous studies (Defraeye et al., 2024; Getahun et al., 2017a) have only considered 2D models or did not include the refrigeration unit explicitly.

This study aims to develop and validate a CFD model that characterises the airflow and heat transfer inside a refrigerated container

packed with ventilated packaging for citrus fruit. An RC is selected that is loaded with citrus fruit palletised in A15C-SV packaging, a configuration that represents roughly 50 % of South African citrus container exports. To tackle a key limitation of the previous simulation studies, a unique feature is the experimental characterisation and implementation of the refrigeration unit (fan and cooling) in the CFD model.

By accurately simulating the cooling processes, the aim is to identify potential regions susceptible to chilling injury, which can significantly impact fruit quality. Insights from the results will further be used to formulate improved approaches for monitoring commercial containers and to guide future research on mitigating chilling injury risks, thus providing valuable guidance for industry practitioners to enhance temperature monitoring practices and reduce food waste.

2. Materials and methods

2.1. Computational model and simulation

2.1.1. Model geometry

An ISO-compliant Refrigerated Intermodal Container classified as a Series 1 freight container with an external height of 2.90 m (high-cube), was employed in this study ([International Organization for Standardization \(ISO\), 2018](#), [International Organization for Standardization \(ISO\), 2020](#)). The Maersk unit measured 12.19 m (40 ft) in length (dimensions listed in [Table 1](#)), exceeding the standard external height of 2.59 m for Series 1 containers. This container's specifications represent those most commonly used in fresh fruit export industries. Airflow rates in RCs vary widely, generally depending on the make and condition of the refrigeration unit (RU). Specifically, container flow rates have been reported to range between 1000 and 8000 m³ h⁻¹ ([Defraeye et al., 2024](#); [GDV, 2012](#)). The unit and condition used in this study were relatively modern and new, thus operating at the higher end of this range.

The RC has a T-bar flooring system, as shown in [Fig. 1](#). There were 35 T-bar extruded surfaces that run along the floor (x-axis) from the refrigeration unit up to the door. The container uses a bottom air delivery system to circulate cold air through the T-bar floors to the palletised fruit. [Fig. 2](#) illustrates the air circulation mode inside a RC equipped with a bottom air delivery system. The refrigeration unit was a Carrier Transicold PrimeLINE system.

The container was fitted with a void plug, typically made from corrugated paperboard, represented as narrow (10 mm) gaps in the simulations. Strategically located at the container's rear ([Fig. 3](#)), the plug was positioned between the final pallets and the door, covering the exposed T-bar floor and the pallet bases. Its primary function was to improve cooling efficiency and uniformity by directing airflow and acting as a barrier to prevent air from bypassing the pallets and returning directly to the plenum. A deliberate gap of approximately 100 mm remains between the container door and the void plug, allowing a controlled amount of cool air to ascend along the less insulated door and dissipate heat ingress ([Lukasse & Snels, 2022](#)). Additionally, a red line marked by the manufacturer traces the top of the side walls and descends near the door, a guideline typically required by shipping lines. This line indicates the maximum permissible height and length for loading, ensuring unimpeded return airflow to the refrigeration unit for optimal air flushing within the container, as described by [Scharnow \(2014\)](#).

Table 1

Geometric dimensions of container and pallet domains.

| | Pallets per row | Dimensions (m) (length × width × height) |
|-----------------------------------|-----------------|---|
| Refrigerated container (interior) | | 11.59 × 2.29 × 2.55 |
| Refrigerated container (exterior) | | 12.19 × 2.44 × 2.90 |
| Single pallet stack in left row | 11 | 1.20 × 1.00 × 2.16 |
| Single pallet stack in right row | 9 | 1.00 × 1.20 × 2.16 |

2.1.2. Model setup

The container model was developed as a 3D continuum, finite volume method. Airflow convective heat transfer processes were modelled using the Navier-Stokes equations in combination with the SST $\kappa-\omega$ turbulence model. The model was implemented with three domains: First, a standard fluid air domain was used to represent the free-flow regions around the fruit pallets (supplementary materials: Section S1.1.1). Second, a porous media domain to represent the twenty pallet stacks (two rows as per [Table 1](#)), whereby a two-phase porous model approach (Local Thermal Non-Equilibrium) was employed to simulate convective and conductive heat transfer processes within the pallet stacks. The airflow resistance of the pallets was incorporated using the Darcy-Forchheimer equation, with coefficients determined from experiments (supplementary materials: Section S1.1.2). The third domain was the refrigeration unit, which dynamically regulated airflow and cooling within the model. A unique contribution of this study was the implicit incorporation of the refrigeration unit, which, once validated, can be used to explore alternative container loading scenarios. Given the high overall computational cost of the simulation, the strategy in this study was to select a simplified geometry conducive to implementing the implicit momentum and energy source/sink terms, which is documented in the supplementary materials (Section S1.2).

2.1.3. Refrigeration unit: fans

The fans were included as momentum source terms. Parameters for this implementation were derived from experimental data. The axial fans were implicitly represented in the model by first conducting an axial fan performance experiment on the container's refrigeration unit. Characterisation of the fans was achieved by iteratively modifying the flow rates at the outlet (through physical obstruction) of the refrigeration unit and measuring the reciprocal pressure drop across the unit fan using a pressure differential meter (Air Flow Meter Type A2G-50, WIKA, Alexander Wiegand SE & Co. KG, Klingenberg, Germany). Air velocities were measured at the air return region using an RS PRO RS-90 anemometer (Accuracy: ±3 %; ±0.30 m s⁻¹). The resulting model was incorporated as an expression in the refrigeration unit domain ([Fig. 3](#)), which accounts for the geometry of the fan duct, specifically its length and radius, as well as the fan's flow rate and system curve.

2.1.4. Refrigeration unit: energy heat sink

For the transient cooling process, the cooling capacity of the refrigerated container and the temperature cooling mode were implicitly represented in the model. The cooling capacity of the refrigeration unit was implemented as an energy sink term. According to [Wild \(2014\)](#), the active cooling capacity of a Thermo King Smart Reefer system ranges between about 6 kW and 13 kW. The refrigeration unit in this study was a Carrier system, which was expected to operate in similar cooling capacity ranges. Most RCs use confidential algorithms that regulate the cooling rate to optimise power usage efficiency ([Lukasse et al., 2011](#)). Consequently, most refrigeration units scale cooling performance with increasing/decreasing load ([Wild, 2014](#)).

Experiments evaluating the cooling capacity of the containers were conducted to determine if the parameters provided by [Wild \(2014\)](#) could be applied to the energy sink in the model. A maximum cooling capacity of 14.2 kW was identified for the refrigeration unit (RU) by monitoring the airflow rate and temperature difference between the inlet and outlet when empty (before loading at the Sunday River Citrus Company (SRCC) and during the trial (during cool-down)). The thermal sink was configured to remove energy up to this rate, with the ANSYS CFX Expression language used to monitor the area-averaged temperature across the inlet plane and calculate the appropriate heat sink rate upstream in the RU cylinder domain ([Fig. 3](#)). Energy removal ceased when the outlet temperature was equal or lower than the specified set point.

A sensitivity analysis confirmed the model's independence from timestep size using the following parameters. Initially, shorter 5 s timesteps were applied to resolve the large temperature differences at

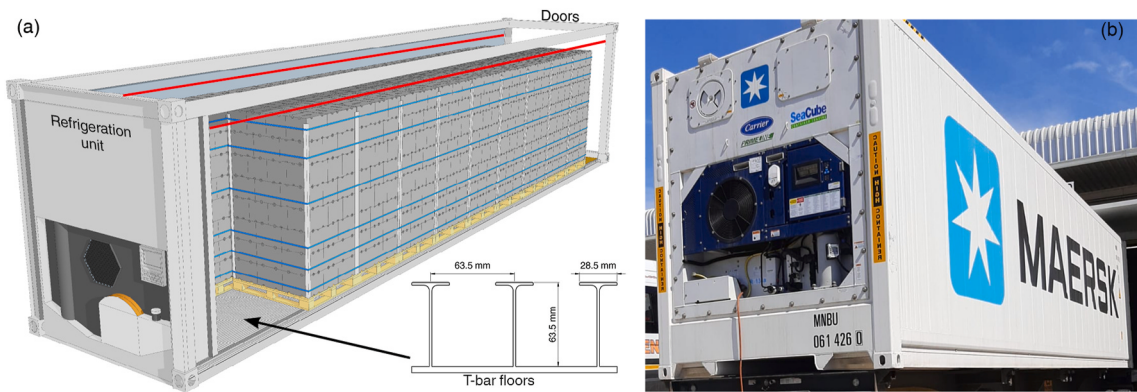


Fig. 1. (a) Refrigerated container with bottom air delivery system used in this study. (b) Photo of the RC (Carrier Transicold Primeline; Container C) used in the validation experiments at Sundays River (South Africa). The red line that indicates the maximum loading height is shown in (a). (For interpretation of the references to colour in this figure legend, the reader is referred to the Web version of this article.)

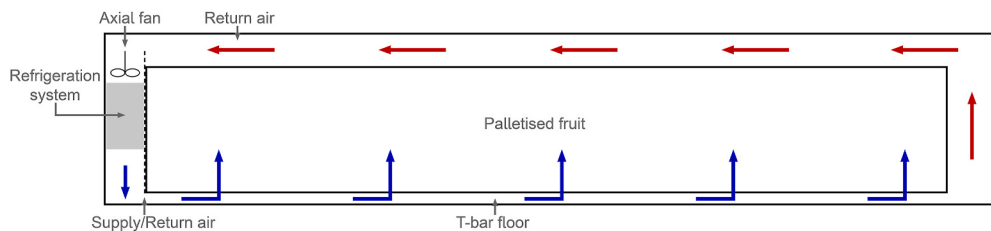


Fig. 2. Schematic illustration of the airflow circulation inside a refrigerated container using a bottom air delivery system.

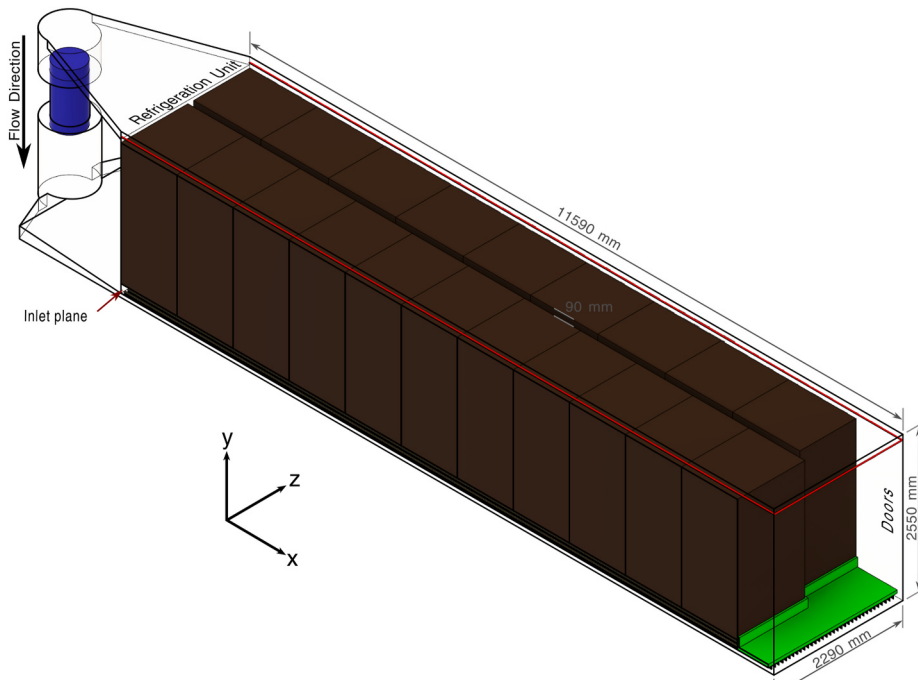


Fig. 3. Fully packed refrigerated container model. Brown domains indicate pallets, the blue domain indicates the refrigeration unit, the green domain indicates a void plug, the red line indicates the red line loading limit, and the quasi-transparent domains show free air zones. Industry-accepted vocabulary for containers is as follows: Regions near the refrigeration unit are the "front", and regions near the door are the "back" of the container. Similarly, there are eleven and nine pallets on the left and right sides, respectively. (For interpretation of the references to colour in this figure legend, the reader is referred to the Web version of this article.)

the simulation's start. As the larger temperature differences decreased, the timestep was relaxed to 90 s after 1 h and 180 s after 10 h.

2.1.5. Model initialisation

The model's initial conditions were set to replicate the experimental

container used for validations. The exterior temperature was set to 20 °C to match the mean outside temperature during the experimental validation. The container's set point was initially at 2 °C for 53 h and then, on the request of the exporter, was adjusted to 3 °C to help mitigate the risk of chilling injury due to prolonged exposure to low temperatures.

2.2. Fruit and packaging boxes

Citrus Navel oranges fruit (*Citrus sinensis* (L.) Osbeck) were packed in A15C-SV cartons (Fig. 4), which were stacked on a standard pallet (1.2 × 1.0 m). Sixty-four fruit were packed in each carton, with an average diameter of 79 mm. The average mass of each pallet stack was approximately 1200 kg and carried 80 cartons. Photos of the pallet stack arrangements during the experiment container loading are shown in Fig. 5.

2.3. Validation experiments

The RC validation experiments were conducted at the Sunday River Citrus Company (SRCC) in Kirkwood, South Africa, in May 2020. The SRCC generously supplied an RC and its fruit for four days before the container was to be shipped. Characterisation experiments were performed on the RU before the fruit were loaded, and all remaining airflow and cooling experiments were performed once the container was loaded.

2.3.1. Air speed measurements

Candlestick sensors (Advanced Thermal Solutions Inc, Norwood, MA, USA), with an air temperature accuracy of ±1 °C and air speed accuracy of ±2 %, were used in conjunction with a TVS 1100 Datalogger to measure non-directional air speeds at various regions in the RC. Measurements were taken at multiple regions in the container, with an

emphasis on regions between the pallet stacks and the container ceiling and between the pallet stack and the container door (Fig. 6).

2.3.2. Temperature measurements

Fruit and air temperatures in the container were measured at 42 positions using both probed and ambient temperature loggers (Tinytag Plus 2 – TGP-4510, Gemini Data Loggers, UK, range: 40 to +85 °C, accuracy: ~0.35 °C). Pulp and air temperatures were monitored at 10 min intervals throughout the 96 h experiments. The thermostat of each probe was located at the tip of a 100 mm long, 4 mm thick stainless-steel spike. Each probe was fitted with a 3D-printed spacer at the probe's base to limit its length to just 50 mm, improving accuracy during probe insertion. For pulp temperature measurements, the probe tip was inserted ~10 mm off-centre into the fruit flesh, positioned within the fleshy segment. The probed fruit and air temperature sensor were both placed at least 150 mm inside the carton to ensure representative air temperature readings. Companion air sensors were positioned within 200 mm of the probe, in the same carton.

Placement of probes was strategic, targeting pallets R01, R03, R06, R09, L02, L05, and L10. Within these pallets, sensors were located explicitly at both the top and bottom layers of the centres, midlines and sides, as depicted in Fig. 6. An air sensor logger was placed outside, in the shade of the container, to record ambient air temperatures. Detailed descriptions of the error calculations are available in the supplementary materials (Section S1.5).

Direct comparisons of experimental and simulated temperature data for validation analysis were achieved by converting the data into a dimensionless scale (Y), where the initial temperature was set to 1.0 and the target temperature (2 °C) to 0.0. This approach effectively normalises minor differences in temperature between the modelled and measured temperatures at specific points, thereby improving the analysis of cooling patterns. The supplementary materials (Section S1.5) contain supporting information for this method.

2.4. Container loading

The pallets were loaded into the container using a forklift, and the process lasted ~1 h. Pallets were installed with temperature loggers before loading to not disrupt the process. In the model, pallets were positioned flush against the container's side walls, as depicted in Figs. 3 and 5, creating a 90 mm gap between the two rows. In practice, pallets tend to lean slightly, as illustrated in Fig. 5, which could result in small gaps of varying size. The forklift drivers were instructed to position the pallets against the walls during the experiment, a common practice in the industry. Consequently, in the CFD model, the pallets were considered to be in direct contact with the container walls. Once loaded, the container doors were immediately closed, and the refrigeration unit was activated.

3. Results and discussion

3.1. Refrigeration unit axial performance curve

Fig. 7 shows the experimental characterisation of the axial fan performance curve and the corresponding function. The resulting function was implemented as a momentum source using the ANSYS CFX Expression language, which enabled the model to react dynamically to the pallets loading in the refrigeration container.

3.2. Airflow validation and in-container flow analysis

3.2.1. Model validation: Airflow

The air speed behaviour within a simulated 3D refrigerated container was compared against that of a full-scale, commercially loaded container. Fig. 8 shows a comparison between the measured and simulated air speed values. In the overhead region (L04, L09, L10, R02, R06)

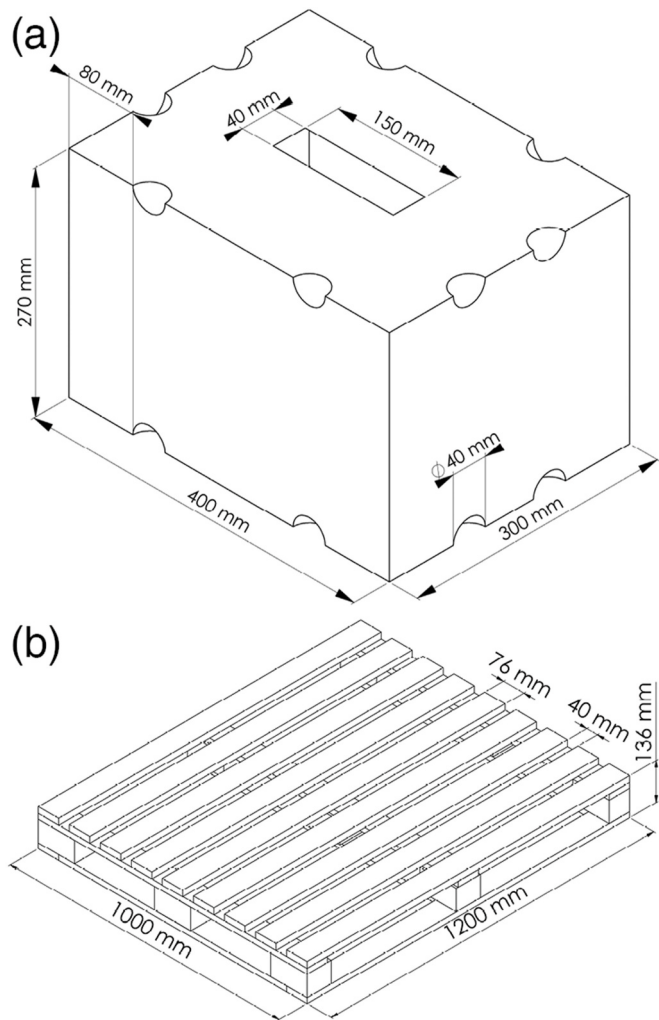


Fig. 4. Schematic diagram of the (a) Supervent carton (A15C-SV; ~15 kg) and the (b) pallet base used in the validation experiments.



Fig. 5. Photographs demonstrating pallet arrangement inside the refrigerated container. Image (a) illustrates the variability in the gap between pallet stacks and their alignment relative to the container wall, highlighting non-uniform spacing. Image (b) depicts a pallet positioned at an angle, creating a noticeable lean away from the container wall.

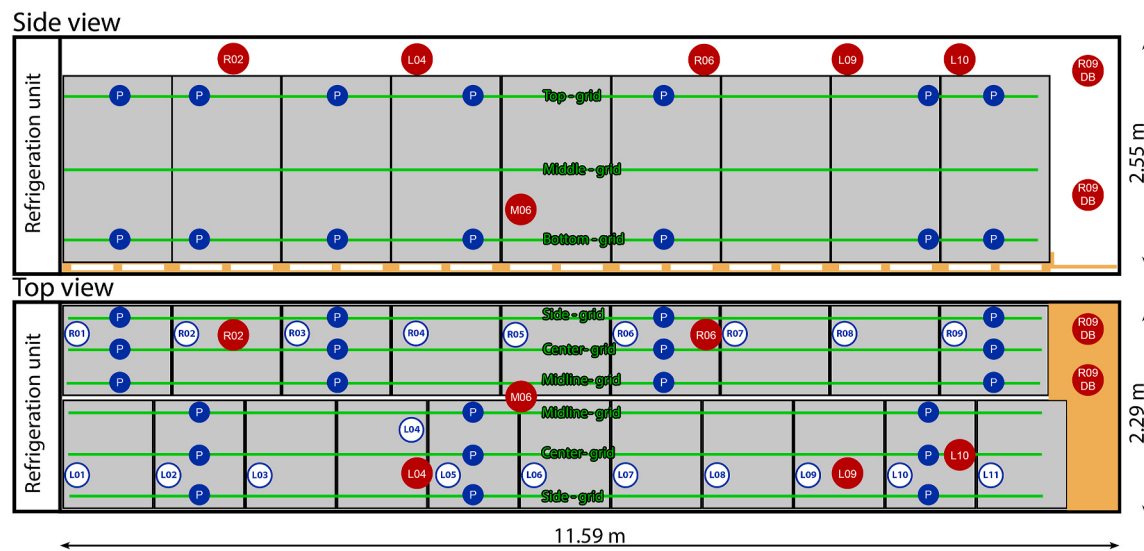


Fig. 6. Schematic of the refrigerated container showing air speed sensor placements (red circles) and the temperature logger positioning (solid blue circles). The green lines form a matrix used for positional referencing during analysis. Blue numbers in white circles show the pallet ID. The brown plane at the door represents the void plug. (For interpretation of the references to colour in this figure legend, the reader is referred to the Web version of this article.)

above the pallets, the model exhibited an average error of 6 % (symmetric mean absolute percentage error (sMAPE; supplementary materials: Section S1.5) relative to experimental measurements, satisfactorily capturing the airflow escaping the pallets and returning to the container's refrigeration unit. This error was good compared to earlier modelling approaches validated in these regions (Getahun et al., 2017a; Hoang et al., 2015; Mourah et al., 2009). However, the gap between pallet stacks (M06) showed a larger prediction error of 35 %. This is likely attributed to the over-simplified geometry of the pallet stacks in the simulation when compared to the experimental pallets, which have an uneven surface from the individual carton faces that are not perfectly aligned, as shown in Fig. 5. These uneven surfaces likely contributed to some unpredictable airflow patterns within the gaps, making validation in this region challenging and foreshadowing the significant impact of

gaps on cooling performance, which will be addressed in more detail in the subsequent cooling discussions. Note that, as with most airflow experiments, the air speed magnitude was known but not the direction.

The largest differences were observed at the door region (R09DT and R09DB), with a predictive error of 56 % (sMAPE). Similar to the gap region, this area was likely also too idealised in the model. Fig. 9 illustrates a jet of air exiting the gaps between pallets towards the door and a stream of air entering between the void plug and door with velocities ranging from 0.4 to 0.7 m s⁻¹. Geometric variances in the pallets and void plug likely influenced the airflow distribution, the speeds of which were in line with the experimental monitors. However, as the bulk of the air in the door region circulated back to the refrigeration unit without passing through the pallets, its influence on fruit cooling performance was minimal.

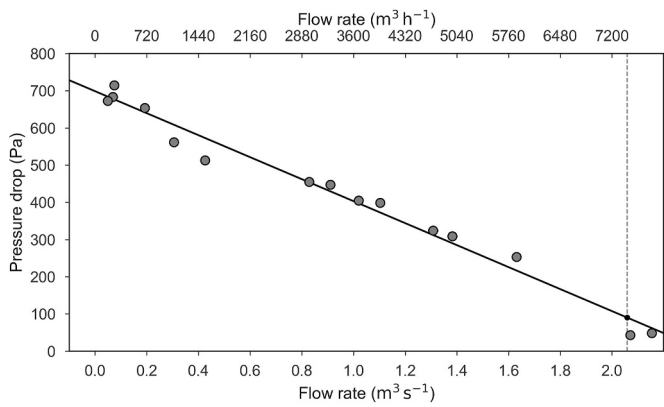


Fig. 7. Axial-fan performance curve determined experimentally (●) and the linear fit implemented in the CFD model ($\Delta P = -296 Q + 699; R^2 = 0.98$). Flow-rate ($Q; \text{m}^3 \text{s}^{-1}$) is given on the bottom x-axis in SI units ($\text{m}^3 \text{s}^{-1}$) and, for industry reference, on the top axis in $\text{m}^3 \text{h}^{-1}$ (conversion factor = 3600). The vertical dashed line marks the container's working point ($2.06 \text{m}^3 \text{s}^{-1}$ or $7412 \text{m}^3 \text{h}^{-1}$). Each marker represents a single measurement; no replicate data were available, so error bars are not shown.

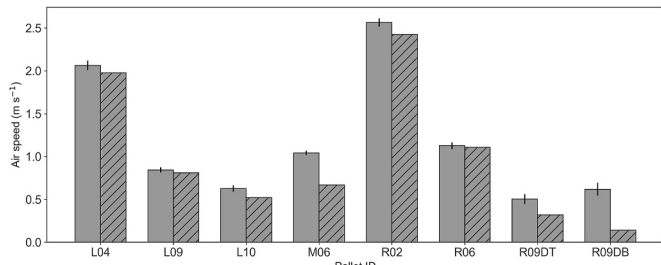


Fig. 8. Experimental (solid grey) and numerical-model (hatched grey) air speed results for the validation container. Error bars denote the standard deviation of the mean.

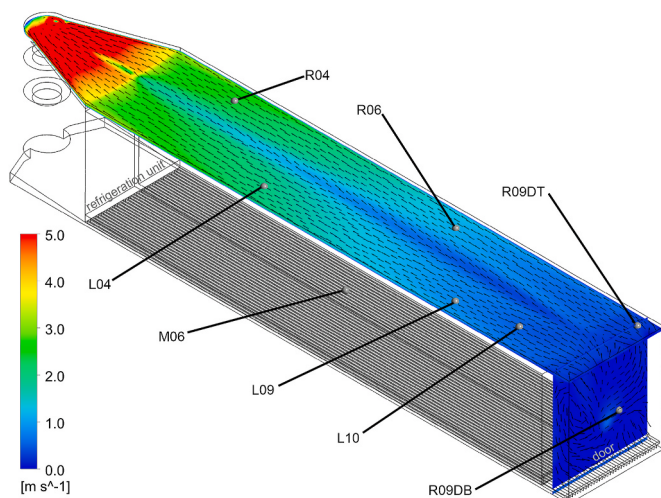


Fig. 9. Velocity magnitude contour plot with vector arrows through planes intercepting the air speed validation points (as indicated in Fig. 6).

The results demonstrated that the numerical model satisfactorily predicted air speed distributions within the RCs. However, a limitation arose in the validation process due to the inability to place candlestick probes within the tightly packed cartons; attempting to do so risked damage to the delicate sensors. This challenge has been a recurrent issue

in validating RC simulations (Getahun et al., 2017a; Moureh et al., 2009). A viable approach to address this could be the adoption of scaled-down experimental models. However, this study also utilised temperature logger data to verify the model's accuracy in simulating heat transfer between the air and the fruit, which was intrinsically linked to the airflow distribution and velocity within the porous structure of the pallets.

3.2.2. Airflow distribution and rates in the air gaps of the container

The airflow distribution within the container was predominantly determined by two factors: the spatial configuration of the pallets and the respective airflow resistance coefficient (ω) of the pallets (supplementary materials: Section S1.1.2).

The airflow rate through the refrigeration unit was predicted to be $7412 \text{ m}^3 \text{ h}^{-1}$ (Fig. 7). Fig. 10 illustrates the airflow conditions in the region between the two pallet rows. The gap between the two pallet rows had a mean air speed of 0.5 m s^{-1} and a maximum of 5.8 m s^{-1} at the inlet. Notably, 14 % of the total airflow, or $980 \text{ m}^3 \text{ h}^{-1}$, was escaping from the top and back regions of the gap, while another $301 \text{ m}^3 \text{ h}^{-1}$ or 4 % of the flow, escaped from the T-bar floor at the region between the void plug and door. This indicated that 82 % of the airflow supplied by the refrigeration unit was channelled through the palletised fruit.

The predominant direction of airflow within the gaps between pallets was upwards. Closer to the refrigeration unit, the air was observed to flow diagonally upwards towards the unit, as depicted in Fig. 10, while air near the door exhibited a diagonal upward trajectory towards the door. A pronounced recirculation zone of airflow within the pallet gaps, in proximity to the refrigeration units, was predicted, aligning with observations from Defraeye et al. (2022, 2024) and is discussed further in section 3.2.4.

3.2.3. Airflow distribution within pallets

Fig. 11 shows the velocity and pressure contours along the container's length, with vector arrows indicating the airflow distribution throughout the space. The overall air velocity in the container diminished as the distance from the cooling unit increases, which corroborated findings reported in the literature (Defraeye et al., 2023, 2024; Getahun et al., 2017a; Issa & Lang, 2016; Moureh et al., 2009; Senguttuvan et al., 2020, 2021). Notably, pallets closer to the cooling unit experienced twice as much air penetration ($0.16\text{--}0.12 \text{ m}^3 \text{ s}^{-1}$ per pallet) than those positioned near the door end ($0.084\text{--}0.048 \text{ m}^3 \text{ s}^{-1}$ per pallet). This pattern aligns with industry observations, which indicate enhanced cooling rates and thus increased susceptibility to chilling injury in pallets closer to the refrigeration unit, as opposed to pallets closer to the door.

As depicted in Fig. 11, a pressure loss gradient was present throughout the length of the container. The initial pressure drop caused by the refrigeration unit amounts to 90 Pa , a value extracted from the model (Fig. 7) and determined by the air recirculation rate. A predicted pressure loss of 32 Pa occurred between the inlet and outlet regions. The air movement within the cargo hold, directed from the inlet towards the door, was driven by an 11 Pa pressure differential. Its recirculation to the outlet was caused by a more substantial differential of 21 Pa . The contribution to pressure loss from the T-bar floor was minimal, while the pressure drop across the top and bottom surfaces of the pallets was relatively low, ranging from 1 to 4 Pa . A notable feature of this model was the use of an implicit refrigeration model, however, the momentum losses caused by the refrigeration unit, which are theoretically assumed to be substantial, were not separately accounted for in this work; instead, the unit's fan system was evaluated experimentally as a whole, thus encompassing all the gains and losses as an aggregate measure.

The pallet stacks' airflow resistance characteristic (ω) represents an experimentally determined aerodynamic resistance. This resulted from obstructions and flow geometry within the pallet system, significantly influenced airflow distribution inside the container. A disproportionately low ω along the horizontal axis compared to the vertical axis

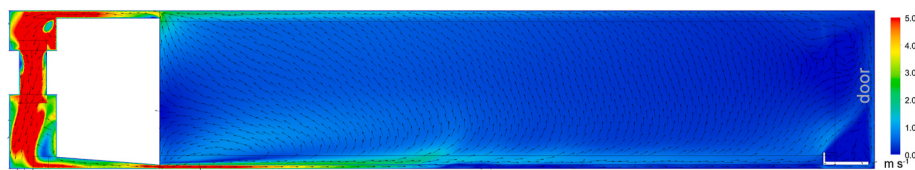


Fig. 10. Velocity magnitude contour plot with vector arrows at the freestream region between pallet rows.

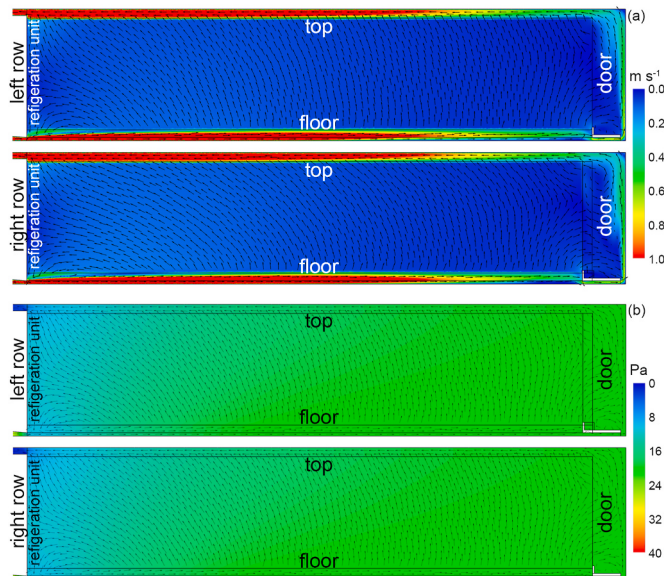


Fig. 11. Contour plots of simulated air velocity magnitude (m s^{-1}) (a) and static pressure (Pa) (b) along the longitudinal centre of the left and right pallet rows (centre grid plane in Fig. 6), with arrows indicating airflow direction.

caused more air to be diverted horizontally, reducing vertical airflow. A sensitivity analysis examining the effect of the ratio between the vertical and horizontal ω of the pallets, performed by Tiamiyu (2020), revealed a pivotal transition point: when the pallet ω ratio (vertical to horizontal) reached approximately 0.4, and a marked increase in vertical air velocity across the pallet height was observed. This finding has significant implications for ventilation design in fresh produce packaging and represents a key area of continued research. Fig. 11 further illustrates a more vertical airflow vector in the left row compared to the right row, attributable to distinct horizontal airflow resistance coefficients (ω) applied during the sensitivity analysis phase of model development (supplementary materials: Table S1).

Flow vectors in Fig. 11 and velocity profiles in Fig. 12 revealed distinct airflow patterns within the container. Airflow primarily ascended vertically, with horizontal deflection towards the void space near the door and diagonal upward flow near the cooling unit. Velocity ranged from 0.03 m s^{-1} to 0.16 m s^{-1} , with air transit times from the base to the top of a pallet varying between 2.0 and 0.2 min, which was an order of magnitude slower than typical rates in forced-air cooling tunnels (Berry et al., 2022; Thompson, 2004). The average particle Reynolds number in palletised areas was 466 (Fig. 12), indicating transitional airflow between laminar and turbulent states, based on standard fluid dynamics through packed beds, where laminar flow ceases at particle Reynolds numbers above 10 and becomes fully turbulent beyond 2000 (Rhodes, 2008).

Distinct airflow zones were observed along the container length: a recirculation zone within the first 2 m, a stabilisation zone from 2 to 5 m with consistent direction and speed, and a vertical flow zone beyond 5 m, where velocities gradually decreased to around 0.04 m s^{-1} at the last pallet. Airflow accelerated slightly in the final metre of the pallet stack,

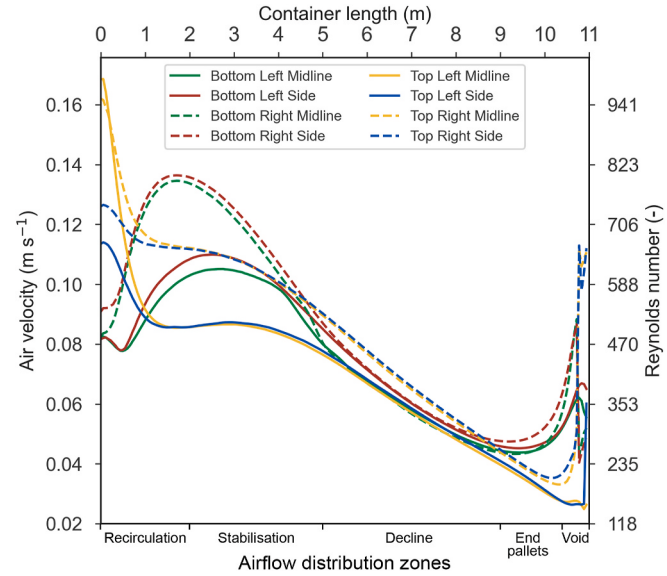


Fig. 12. Simulated air velocity profiles (left axis, m s^{-1}) along eight longitudinal lines through the pallet stack; transect positions are those highlighted in green in Fig. 9. The right axis re-expresses the same data as particle Reynolds number ($\text{Re} = \rho d u / \mu$), so velocity and Re are linearly related. Colours identify the paths: green = bottom midline, yellow = top midline, red = bottom side, blue = top side; while dashed curves trace the right-hand pallets and solid curves the left-hand pallets. The lower abscissa shows the airflow zones discussed in the text. (For interpretation of the references to colour in this figure legend, the reader is referred to the Web version of this article.)

likely due to increased exposed surface area, before exiting along pallet boundaries and gaps. The final 0.6 m above the void plug exhibited heterogeneous air movement.

3.2.4. Recirculation zone

A recirculation zone is evident at the bottom of the first two pallets nearest the refrigeration units (Fig. 12). This complex recirculation pattern is evident ($\leq 2 \text{ m}$ from the refrigeration unit) as a low air velocity zone in the middle regions and variable flow rates in the top and bottom regions. The recirculation zone near the refrigeration unit is explored in Fig. 13a. This zone was initiated by the sudden expansion in volume from the inlet duct into the container loading space. The Coanda effect caused air to "attach" to the duct's top and the container's bottom walls, by which the airflow jet cannot directly make the turn upwards when exiting the inlet duct. The resulting wall shear (due to no-slip) created a sudden flow separation at the expansion, as seen in Fig. 13b. The resulting vortex was enhanced by the turbulent wake flow, which experienced vertical momentum as it became fully turbulent and unstable (Defraeye et al., 2022).

A potential solution to reduce the recirculation zone is to direct the fluid momentum on the bottom wall of the duct such that the fluid profile remains more stable in the expansion region. This can also manipulate the turbulent wake region to develop further along the length of the container, thus restricting its contribution to the backflow, which was observed. For instance, Defraeye et al. (2024) showed that

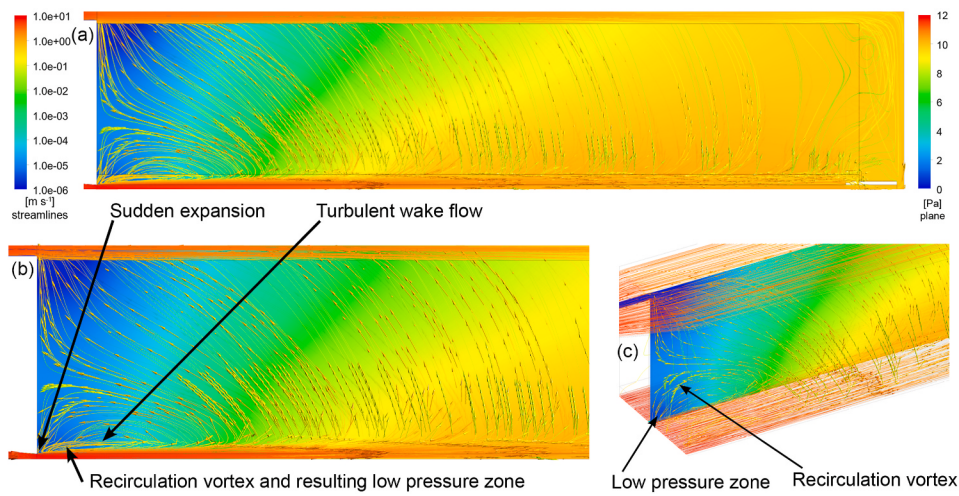


Fig. 13. CFD visualisation of airflow in the 90 mm gap between the two citrus pallets in the container. The colour map shows pressure (Pa) along the plane in the middle of the respective air gap; streamlines released from the refrigeration unit outlet are coloured by air velocity magnitude (m s^{-1}). (a) Entire plane viewed from the side wall (refrigeration unit left, doors right). (b) Magnified image of the refrigeration unit end, highlighting the low-pressure recirculation cell. (c) Oblique top-left view of the same region, emphasising the three-dimensional roll-cell structure. (For interpretation of the references to colour in this figure legend, the reader is referred to the Web version of this article.)

lengthening the T-bar floor can reduce the predicted recirculation zone. One alternative approach is to direct the refrigeration unit's flow along a soft curve to ensure a greater downward flow momentum. Alternatively, a sheeting material could be applied along the top of the T-bar floor to modify the airflow distribution. These proposals are speculative, and it is expected that the recirculation zone will be highly sensitive and that minor manipulations could change its location in the container and ease the effect. However, in all cases of a sudden expansion, creating a vortex is inevitable, and only the location and severity can be modified. These simulations raised several important questions, such as (i) how accurately the severity of the recirculation is predicted and (ii) to what extent the recirculation can be mitigated or even if it should be a priority. Defraeye et al. (2022) further discussed the recirculation zone, and further work exploring these concepts is currently underway.

3.3. Model validation: cooling profiles

3.3.1. Model validation: Cooling

The average cooling profiles for the monitored positions, as depicted

in Fig. 14a, demonstrated a good predictive agreement, with the mean coefficient of determination (R^2) reaching 0.93. The CFD numerical approach applied in this study demonstrated reasonable accuracy in capturing the experimental cooling processes. Nonetheless, two main variances were identified between the simulation and the experiment (Fig. 14a). Initially, there was a discrepancy in the starting temperatures, where the average pallet temperature was recorded at 17.6 °C, but the mean temperature measured by the probes was approximately 2 °C lower. Another variance was observed in the equilibrium temperature. The experimental container's thermostat (set point) was adjusted from 2 °C to 3 °C after 53 h to minimise the risk of chilling injury to the commercial fruit, a modification not mirrored in the model to maintain a focus on the initial cooling profiles.

A notable discrepancy between simulated and experimental data was observed in the inlet (delivery) and outlet (return) air temperatures (Fig. 14b). Air speed validations confirmed that the model accurately represented the flow rates through the refrigeration unit, and Fig. 14a demonstrates that the model successfully replicated the mean cooling rates within the experimental container. The model heat sink term thus

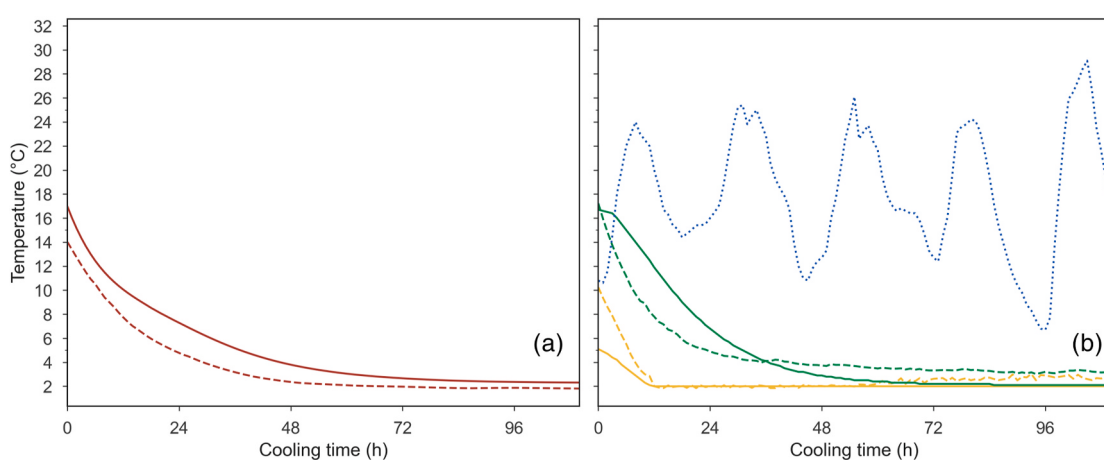


Fig. 14. Comparison between the experimental trial and CFD simulation for (a) the mean fruit pulp temperature across all probe positions, and (b) the inlet (delivery) and outlet (return) air temperatures. In both panels, the solid red line represents the numerical result, and the dashed red line represents the experimental result. In panel (b), the yellow lines show inlet temperatures, the green lines show outlet temperatures, and the dotted blue line shows ambient experimental temperature. The container's experimental set point was increased to 3 °C after 53 h. (For interpretation of the references to colour in this figure legend, the reader is referred to the Web version of this article.)

closely replicated the container's refrigeration coils. Fig. 14b shows that the difference between the simulated and experimental return temperatures was largest over the first 24 h, but differences never exceeded 4 °C. In contrast, the simulated supply temperature started 5 °C lower than the experimental supply, but both reached the set point simultaneously (after 12 h). These findings raise several questions regarding the algorithms governing refrigerated cooling performance, which are not publicly documented, and suggest that the cooling efficiency of the unit

may have increased automatically during the cool-down process.

Fig. 15 illustrates both the experimental and computational profiles of pulp temperature at key locations within the container, as detailed in Fig. 6 and Table 2 lists the corresponding coefficients of determination (R^2) for each case. The differences between experimental and numerical pulp temperatures were in the same range as those found by Defraeye et al. (2024). However, research by Berry et al. (2021) indicated that significant variations in cooling rates can occur among containers

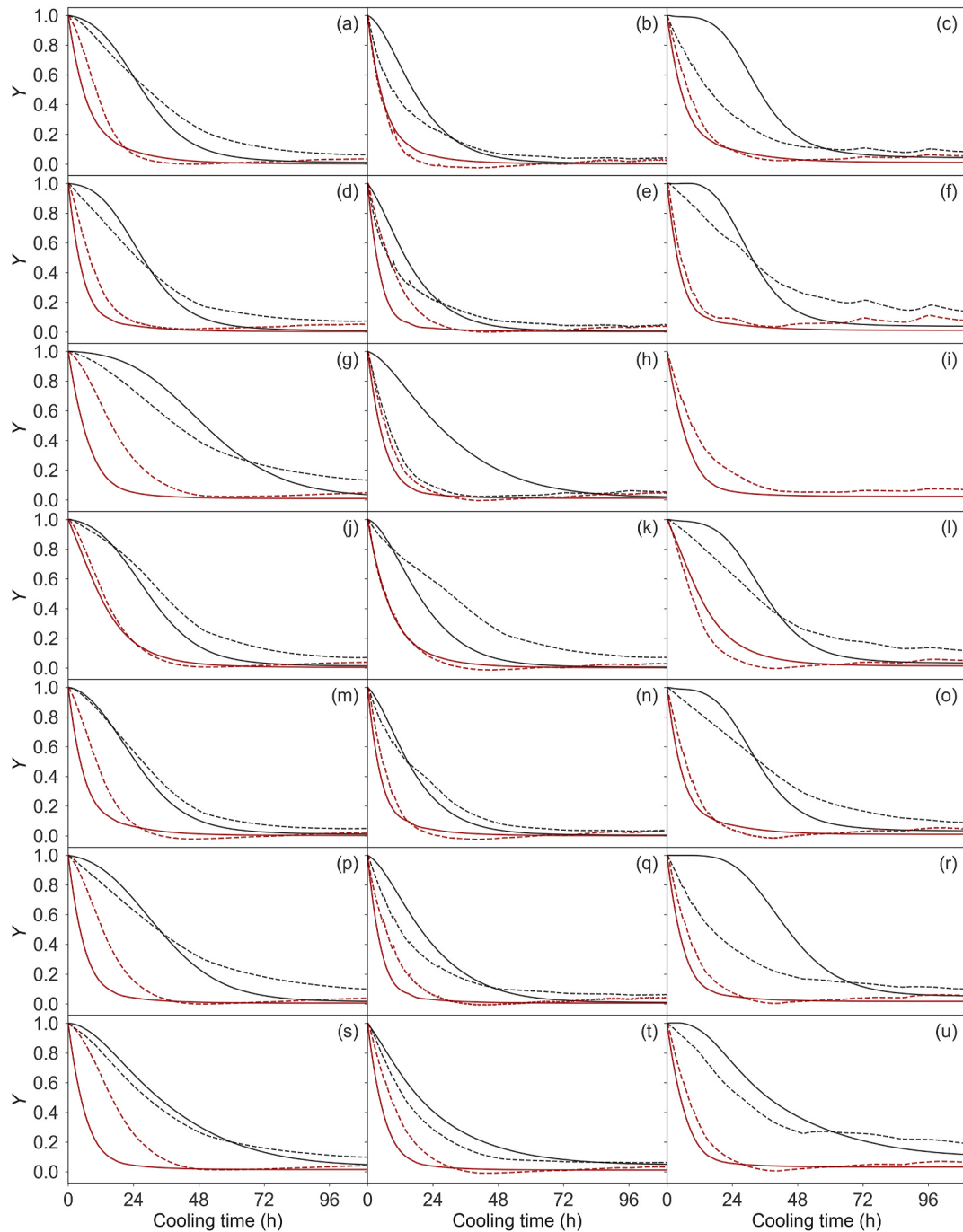


Fig. 15. Fruit dimensionless temperature ($Y = (T_p - T_a)/(T_i - T_p)$) cooling curves for seven monitored pallets at three lateral positions. Panels are arranged by pallet (rows) and position (columns): (a) L02 centre, (b) L02 midline, (c) L02 side; (d) L05 centre, (e) L05 midline, (f) L05 side; (g) L10 centre, (h) L10 midline, (i) L10 side; (j) R01 centre, (k) R01 midline, (l) R01 side; (m) R03 centre, (n) R03 midline, (o) R03 side; (p) R06 centre, (q) R06 midline, (r) R06 side; (s) R09 centre, (t) R09 midline, (u) R09 side. For all panels, solid lines represent the numerical results, and the dashed lines represent the experimental results. Black lines represent top probe data, and red lines represent bottom probe data. The coefficient of determination (R^2) for each top and bottom-probe comparison is listed in Table 2. Note that the experimental container's setpoint was increased from 2 °C to 3 °C, after 53 h. Refer to Fig. 6 for probe positions. (For interpretation of the references to colour in this figure legend, the reader is referred to the Web version of this article.)

Table 2

Coefficient of determination (R^2) values comparing experimental and simulated dimensionless temperature profiles for each subplot in Fig. 15. Each row corresponds to a panel in the figure (a–u), covering all monitored pallets and their lateral positions (centre, midline, side). Missing data are indicated with ‘na’.

| Pallet-position | Panel | R^2 (top) | R^2 (bottom) |
|-----------------|-------|-------------|----------------|
| L02 centre | (a) | 0.99 | 0.95 |
| L02 midline | (b) | 0.96 | 0.97 |
| L02 side | (c) | 0.82 | 0.97 |
| L05 centre | (d) | 0.99 | 0.93 |
| L05 midline | (e) | 0.96 | 0.87 |
| L05 side | (f) | 0.97 | 0.97 |
| L10 centre | (g) | 0.95 | 0.80 |
| L10 midline | (h) | 0.64 | 0.97 |
| L10 side | (i) | na | 0.94 |
| R01 centre | (j) | 0.99 | 0.99 |
| R01 midline | (k) | 0.92 | 0.99 |
| R01 side | (l) | 0.97 | 0.93 |
| R03 centre | (m) | 0.99 | 0.90 |
| R03 midline | (n) | 0.98 | 0.96 |
| R03 side | (o) | 0.97 | 0.96 |
| R06 centre | (p) | 0.99 | 0.82 |
| R06 midline | (q) | 0.96 | 0.91 |
| R06 side | (r) | 0.71 | 0.95 |
| R09 centre | (s) | 0.99 | 0.74 |
| R09 midline | (t) | 0.97 | 0.91 |
| R09 side | (u) | 0.93 | 0.95 |

loaded identically, highlighting the inherent variability in cooling dynamics. This variability stems from inevitable discrepancies in palletisation and loading practices, leading to non-ideal geometric configurations within the container. Factors, such as pallets pressing against the container's walls or uneven pallet stacking, can introduce unexpected gaps or restrictions, altering the cooling airflow path to favour certain pallets over others. Documenting these geometric inconsistencies during the loading process poses a significant challenge, making their exact replication in CFD models impractical. Despite these differences, consistent cooling trends were anticipated across multiple identical containers, such as faster cooling rates at the lower sections of pallets compared to their upper sections. Therefore, the simulation is expected to capture a generalised citrus container cooling trend.

The correlation analysis in Table 2, comparing the experimental and computational results of Fig. 15, demonstrates good predictive modelling accuracy. The highest mean R^2 values were obtained at the top-centre positions (≈ 0.99), the bottom-side positions (≈ 0.95) and the bottom-midline positions (≈ 0.94). Slightly lower correlations were observed at the top-midline positions (≈ 0.91), the bottom-centre positions (≈ 0.88) and the top-side positions (≈ 0.90). Three predictive discrepancies of interest were identified, which provided some insights into possible model improvements in the future:

1. The top-midline sensor at pallet L10 cooled significantly more rapidly than predicted by the model. This sensor appeared to be an outlier, as it was one of the few top sensors that cooled at a rate similar to its corresponding bottom sensor or the corresponding sensors in the adjacent pallets. The rapid cooling observed at this location can likely be attributed to either the improper placement of the sensor device or the local packaging geometry, in which the fruit in this area may have been exposed to a stream of cold air from a nearby vent hole.
2. At the bottom-centres of right-hand side pallets near the door, the experimental fruit cooled unexpectedly slowly compared to the predictions. Interestingly, probe positions (mid-line and side) directly next to these positions cooled similarly to the simulation. This aberration is attributed to the geometry of the packaging, which may have locally insulated the probes near the centre from cooling airflow more than expected when treating the pallet as a porous media. This observation raises an important lesson: although the

simulation accurately captured general cooling trends, it did not accurately predict the non-uniform temperature gradients observed in a real-world container.

3. Several sensors located along the top-side exhibited predictive discrepancies. These anomalies can be attributed to the slightly offset positioning of these pallets from the container's sidewalls, as depicted in Fig. 5b. This offset will likely have diminished heat absorption from the container's walls compared to the simulated and other nearby experimental pallets.

On a practical level, the top-sides of pallets were particularly susceptible to forming gaps, as even a minor lean in the pallet in either direction will distance the top from the container wall, allowing cold airflow to more efficiently remove heat in this region. This dynamic explained why the top-side experimental results (Fig. 15) frequently showed temperatures lower than model predictions, which assumed uniform pallet contact with the container wall. Another factor to consider is the inconsistencies in the gap width between the two pallets. Therefore, the predictive inaccuracies at these locations likely stemmed from the physical setup rather than model inadequacies, suggesting a geometric influence. Future investigations could beneficially explore cooling discrepancies through simulations of containers loaded with irregularly shaped pallets.

The model performance notably surpassed initial expectations, especially when considering the inherent cooling variability observed across identical containers (Berry et al., 2021). The model adeptly captured both the high and low cooling rates observed at the lower and upper regions of the pallets, respectively. Additionally, the total energy extraction, attributed to the implicit modelling of the refrigeration unit, was closely aligned with experimental observations. This indicated that the simulated heat sink capacity of the refrigeration unit was optimally configured. Consequently, the validation of this specific container model demonstrated performance that was on par with, if not superior to, that reported in previous studies (Getahun et al., 2017a; Issa & Lang, 2016; Moureh et al., 2009; Senguttuvan et al., 2021).

3.3.2. Container cooling characteristics

The container in this study was a warm-loaded container, and the cool-down process took between 4 and 6 days to reach stabilisation temperature (T_{eq} ; supplementary material: Eq. (16)), which was consistent with prior studies (Berry et al., 2021; Defraeye et al., 2024). Steady-state conditions in the container were reached when the internal temperature no longer changed, signifying that all thermal processes inside were at equilibrium. Two distinct temperature heterogeneities were observed in the respective container, the first during the cool-down process and the second after the container reaches equilibrium. The distinction between these two unique heterogeneous states has often not been recognised in the literature.

After reaching steady-state, the temperature heterogeneity resulted in the perpetual formation of warmer and colder regions. Warm regions are localised regions with slightly elevated temperatures, potentially leading to accelerated fruit ripening, senescence, and quality deterioration. Conversely, cold spots are regions where the temperature drops below the ideal range, increasing the risk of chilling injury.

It should be noted that real-world containers can operate across different refrigeration modes and are exposed to changing external environments (Fitzgerald et al., 2011), as shown in Fig. 14b, which depicts the external conditions outside the container. Consequently, real-world containers undergo cycles of varying cooling efficiency, causing continuous fluctuations in their thermal steady-state. This variation can position the actual thermal steady-state either below or above the theoretical steady-state, leading to a cooling profile characterised by fluctuations. Therefore, experimentally, the stabilisation temperature (T_{eq}) is regarded as a value closely approximating, but not necessarily always equal to, the steady-state temperature.

Fig. 16 shows the fruit temperatures at several iterations of the cool-

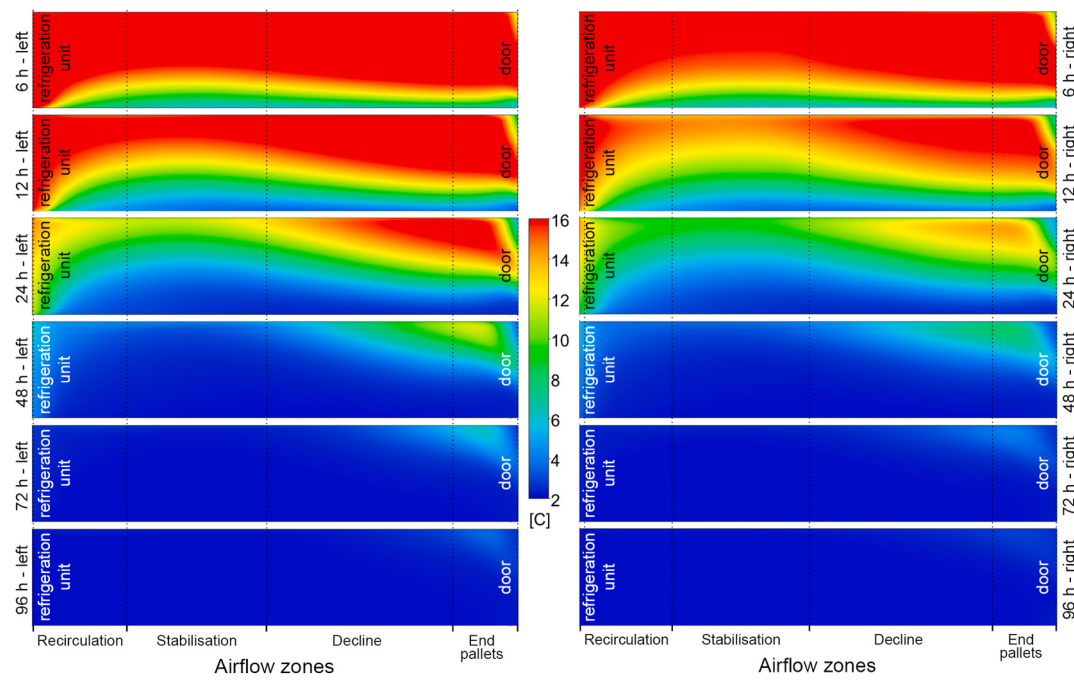


Fig. 16. Simulated temperature contour profile through the middle of the left and right pallet rows at 6 h, 12 h, 24 h, 48 h and 96 h.

down process, which followed a uniquely non-uniform cooling pattern. After 6 h of cooling, the container showed a relatively uniform temperature across its length, with generally warmer temperatures near the doors. After 12 h, fruit within ~2 m of the refrigeration unit and the doors cooled slowest, with the fastest cooling region between 2 and 5 m from the RU. After 48 h, most of the fruit in the container was cooler than 4.0 °C, with a relatively small area at a slightly higher temperature

(warm spot) at the top near the doors. By 96 h, fruit temperatures had largely stabilised as the container reached equilibrium. The coldest region in the container after cool down (~4 days) was at the bottom of the pallets in the stabilisation region. Fruit in this region were exposed to the cold air directly from the refrigeration unit and air speeds in this region were the fastest within the container. Therefore, the highest rates of chilling injury were expected in this region.

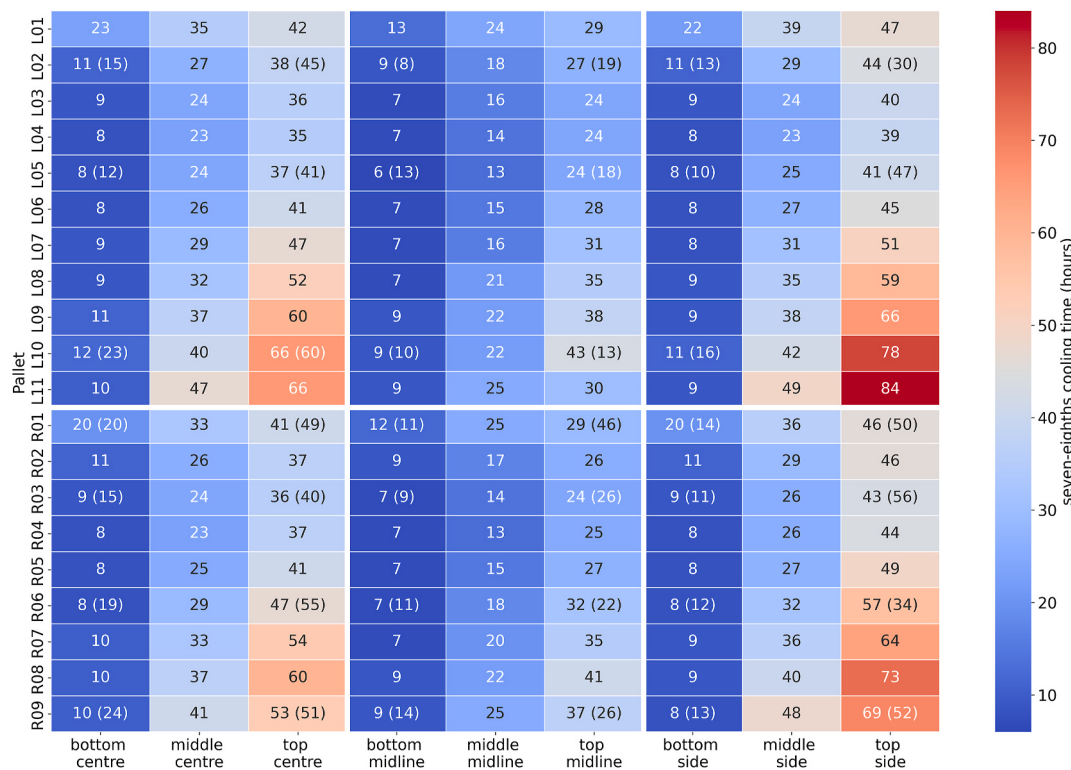


Fig. 17. Heatmap showing the simulated and experimental (in brackets) three-fourths cooling time values for several positions in each pallet within the container. For this simulation, the three-fourths cooling temperature was 5.9 °C.

Notably, the cooling patterns in the container (Fig. 16) follow the airflow zones as proposed in Fig. 12. The fastest cooling zone was within the 'stabilisation' zone. This region, located approximately 2–5 m from the refrigeration unit, is characterised by high air velocities and a predominantly vertical airflow pattern, as illustrated by the velocity vectors in Fig. 11a. The 'recirculation' zone, which initially did not cool very quickly, ultimately had the second fastest cooling rate, followed by the 'declining' zone, and finally, the 'end pallets', which cooled the slowest of all. Predicted airflow and cooling trends in the left and right rows exhibited similar patterns. However, the left pallet row consistently showed a slower cooling rate compared to the right (Fig. 16). Temperature differences were largest initially, with significant differences at localised positions, but these differences narrowed to a mean of only 0.2 °C after 12 h and became negligible after four days.

The spatial cooling heterogeneity of the container is illustrated in Fig. 17, which shows the three-fourths cooling time (TFCT) for each of the 180 intersecting grid lines in Fig. 6. The TFCT is the duration required for fruit at the respective position to cool to 5.9 °C (supplementary materials: Section S1.5). Fruit cooled most rapidly near the bottom of pallets and near the pallet gap (midlines), which follows logically in that these regions were closest to cold air from the refrigeration unit. The TFCT rates in this region ranged between 10 and 21 h. Conversely, the slowest cooling regions were at the top of the pallets nearest the sides, which were predicted to range between 69 and 84 h. From a chilling injury perspective, the bottom midline and centre pallet regions had the highest cooling rates and were, thus, initially the most susceptible to chilling injury-related damage.

Using a porous media model for pallets in simulations may not always optimally predict temperatures near the top of the pallets against the container wall. This discrepancy arose because actual pallets exhibited a lower packing density at the sides and edges, where fruits met the carton and were thus not interlocked with other fruit. In contrast, the simulation model assumed that the porous media was in direct contact with the container wall, neglecting the intervening layer of corrugated paper and the lower packing density of fruit near the edges. Therefore, the model overestimated heat absorption and accumulation into the pallets along the sides. Furthermore, the high probability of gaps between the walls and the tops of the pallets will also diminish heat transfer into these regions.

Consequently, the confidence in the predicted warm spots near the top/sides of the pallets is not very high. However, the overall patterns of temperature profiles within the pallets were accurately represented, as supported by validation experiments. Additionally, the presence of gaps between the wall at either the bottom or top, as illustrated in Fig. 5a and b, can also have a significant contribution.

Cooling profiles in the container were governed by the airflow that predominantly moves vertically through the pallets (Fig. 11). Initially, heat ingress from the container walls, which was dependent on the temperature gradient between the interior and exterior, was not a significant contributor to the cooling process. However, as the internal temperature decreased, the heat transfer rate into the container increased. For instance, net energy absorption started at approximately 61 W but increased to 410 W once the interior cooled to 4.0 °C. This progressive increase in net heat transfer was pivotal to the final temperature distribution within the container, as evidenced by a mean Relative Standard Deviation (RSD) value of 8.5 %, once the container reached steady-state (supplementary materials: Section S2.1). Consequently, these spatial temperature variances can result in uneven fruit quality preservation (Wu et al., 2019, 2019, 2019).

Conversely, heat generated from fruit respiration was more impactful when the fruit were warm, decreasing significantly as the temperature drops, specifically, halving for every 10 °C reduction (Kader, 2002). Given that citrus fruits have notably low respiration rates (4–7 mg CO₂ kg⁻¹ h⁻¹ at room temperature), the effect of cooling on their respiration rate was minimal (Thompson et al., 2008; Vines et al., 1965). However, respiration heat could affect the initial cooling phase and the resultant

temperature profile in containers loaded with high-respiring fruits. Once fruit cool, the influence of internal respiration heat diminished, and external heat ingress became the dominant factor.

3.4. Temperature monitoring in a refrigerated container

4.4.1. Optimal monitoring location for commercial shipments

A key consideration when selecting an optimal monitoring position should be to avoid regions highly susceptible to temperature fluctuations, as these variations could obscure the overall trends within the container. This study, along with previous work by Berry et al. (2021), highlighted that while general temperature trends and patterns were evident, significant temperature variations still existed throughout the container. The highest variability was shown in this study to occur near the top sides of the pallets, where minor changes in gap size between the pallet and the wall significantly influenced the rate of heat absorption and cold airflow reaching the pallet. Although these positions were potential warm spots, their isolated position meant that they provided less valuable information regarding other potential warm or cold spots or about the overall temperature performance of the pallets.

Instead, the results of this study indicated that a more effective approach is to select a more centralised monitoring position influenced by multiple warm regions. Using a more centralised position also allows the user to interpret the respective readings to the other positions in the container. Other important factors to consider include:

1. The temperature of the loaded fruit largely influences the initial cool-down process and results in a unique temperature pattern with warm spots. The selected monitor location should be positioned in a region that can monitor the cool-down process and detect potential heat that may remain from fruit that were not sufficiently precooled. According to Fig. 16, the primary warm regions during the cool-down process are the top two-thirds of the first row next to the refrigeration unit and the top two-thirds of the last two pallets at the back of the container, near the door.
2. After stabilisation (6–7 days), temperature patterns inside the container form a unique distribution of warm and cold spots. The warm spots were most prevalent at the top two-thirds of the last two pallets at the back of the container, near the door. The selected monitor location should thus be positioned in a region influenced by pre- and post-stabilisation warm spots.
3. Installation of the monitor is also an important consideration. Container loading is typically a high-paced process, and there is little capacity to dismantle a pallet to install a monitor. A monitoring device can thus be placed at a maximum of 150 mm into a pallet along any surface of the twenty pallets. However, the most accessible positions for installation and retrieval are at the back of the container on the last pallet surface.
4. Finally, some monitors can transmit data wirelessly. However, the high-water content of the fruit can attenuate these signals. The monitor should optimally be placed on the outer surface of the pallets. The container door is thinner than the container walls and is eventually opened, making a pallet surface near the door the best location for wireless signal transmission.

These four constraints for monitoring positioning indicate sensor placement near the door within the pallets. Fig. 18 shows the pulp fruit temperature distribution within the container during the end of the container cool-down process (after 24 h) and after stabilisation (at 168 h). As previously noted, the left pallet row exhibited a slower cooling rate than the right row. The primary overlap between the warm regions during the cool-down and equilibrium phases occurred at the mid-height of the last pallet and the top of the second-to-last pallet. Although the top sides generally experienced the highest temperatures, these regions have already been ruled out as suitable monitoring locations due to their inconsistent variability and because, experimentally, these regions were

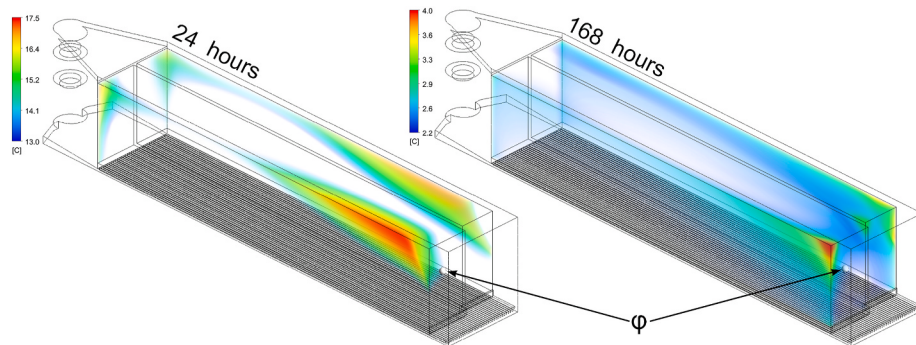


Fig. 18. Volume rendering of pulp fruit temperatures for the slowest cooling regions in the container. Renderings show the warmest regions during the cool-down (24 h) and after the container has thermally stabilised (168 h).

often much colder than in simulations (Section 3.3.1). Given all the constraints, the most optimal placement for a monitor, considering overlapping warm regions, installation accessibility and signal transmission, is ~150 mm into the back of the last left pallet, at the very centre of the pallet face. This location, named ‘ φ ’, captures the critical temperature patterns while allowing for efficient installation and reliable wireless communication. Fig. 19 provides a visual representation of the φ position within the container.

Fig. 20 illustrates the pulp fruit temperatures at φ in contrast to the full range of pulp temperatures recorded at all locations within the container. The predictions demonstrate that the pulp temperatures at the φ position consistently remained within the warmest quantile throughout the cool-down and stabilisation phases. Specifically, after 24 h, the pulp temperature at φ was at the 90th percentile of the warmest positions in the container, and after 168 h, it was at the 87th percentile. This was one of the few positions in the container that captured these higher temperature percentiles for both the pre-and post-stabilisation periods. Therefore, measurements at the φ position effectively captured the warmest temperatures within the container consistently over time. Temperature data from this position were optimally selected to interpret the overall temperature dynamics of the container for this container load-out scenario.

The proposed φ placement offers a strategic approach for monitoring temperatures in refrigerated shipping containers using a single logger device, which aligns with standard commercial practices. While placement φ has been determined explicitly for citrus fruit packed in A15C

cartons within the respective (40 ft) container size, it serves as a foundation for enhanced temperature monitoring across various commodity types and packaging configurations.

3.4.2. Air versus pulp temperature monitoring

Fig. 21 shows the experimental container's temperature differences between air and pulp over time. The air temperature loggers were positioned inside the carton and between fruit. The results showed that the temperature differences decreased rapidly, with the majority of positions reaching a difference of $<0.5^\circ\text{C}$ within 1–4 days. Notably, this difference fell well within the margin of accuracy ($\pm 0.5^\circ\text{C}$) of most commercially used temperature monitoring devices. Similarly, the simulated temperature difference between air and pulp matched the experimental ranges. Specifically, temperature differences for all positions in the simulated container, including φ , were $<0.35^\circ\text{C}$ after 96 h.

The palletised fruit were packed in vented cartons, creating a porous medium that promoted effective heat exchange between the fruit and air phases. The low air velocity (0.03 m s^{-1}) and the pallet height (2.16 m) resulted in an air residence time of over 1 min, allowing sufficient time for heat transfer and equilibration between the fruit and air. These conditions meant that the container rapidly approached a state where the temperature gradients within the porous domains were negligible. This has important implications for temperature monitoring in commercial shipments. It validated using air temperature loggers to monitor fruit temperatures at the optimal φ position.

From a research perspective, when appropriate, installing numerous

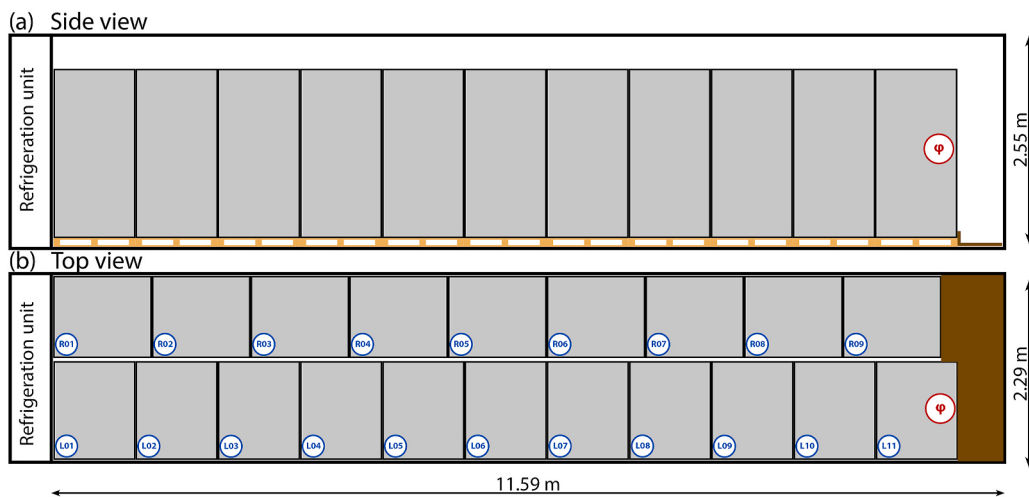


Fig. 19. Side (a) and top (b) views of a fully loaded 40 ft high-cube refrigerated container carrying citrus pallets. Black outlines mark the container walls and pallet edges. Twenty pallets are indexed with blue-circled codes (R01–R09; L01–L11). The proposed single-sensor location φ is on the aft-most pallet at mid-height. Colours: pallets: grey; pallet bases: tan; door-void plug: dark brown. (For interpretation of the references to colour in this figure legend, the reader is referred to the Web version of this article.)

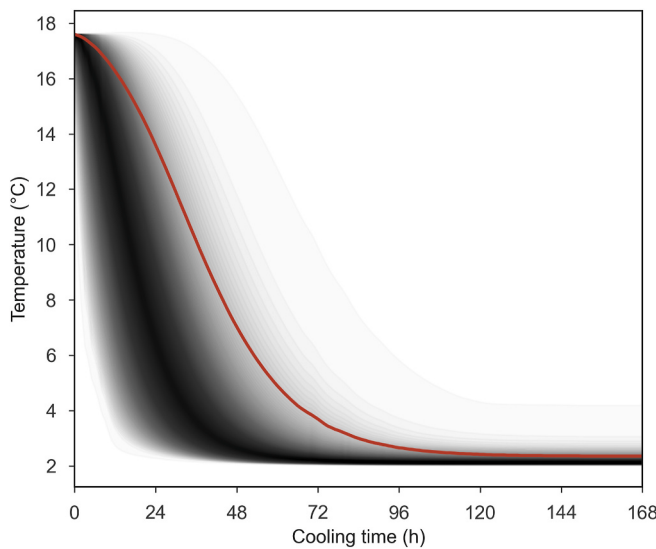


Fig. 20. Cooling behaviour of fruit pulp in the simulated fully loaded 40 ft refrigerated container. Grey density shading depicts the distribution of pulp temperatures at all monitored pallet positions: darker regions indicate a higher proportion of positions occupying that specific time-temperature bin, with contours plotted in 0.5-percentile increments. The solid red curve shows the pulp-temperature history at the proposed single-sensor location φ (aft-most pallet, mid-height). (For interpretation of the references to colour in this figure legend, the reader is referred to the Web version of this article.)

inexpensive air-temperature loggers, supplemented by a few strategically positioned pulp probes, can provide denser spatial sampling without additional cost, enabling a more comprehensive study of temperature distribution and the identification of potential cold-chain breaks.

Although pulp and air temperatures were similar, the Local Thermal Equilibrium (LTE) heat-transfer model, applicable only when the solid (fruit) and fluid (air) phases are at equal temperatures, still did not adequately apply. The Local Thermal Non-Equilibrium (LTNE) approach used in this study was thus valid and necessary. This is motivated by the simulated Biot numbers, which averaged 0.34. Further details on heat

transfer modelling used in this research are provided in the supplementary materials (Section S2.3).

In summary, the experimental results and theoretical analysis demonstrated that the fruit in a refrigerated container reached a state where the thermal gradient between the air and fruit were effectively negligible after ~ 96 h. The results presented here support the use of air temperature loggers at the optimal φ position for monitoring fruit temperatures during commercial shipments. The convergence of air and pulp temperatures means that air temperature sensors can be used as substitutes for pulp temperature sensors, or at least serve as reliable proxies, simplifying temperature monitoring and reducing costs. It provides a reliable approach for ensuring proper temperature management in RC shipments of horticultural products.

4. Future outlooks

This study has provided novel insights into modelling an RC and the cool-down processes of ambient loaded fresh produce during shipping. However, several research questions of interest still need to be addressed. Some questions will require further iterative improvements to the current CFD model to improve prediction accuracy and fully characterise the predictive limits. Specifically, validation experiments with higher-resolution monitoring and especially more extensive replications are needed. This will account for the expected performance variation between individual containers. The RU model can be improved by incorporating a more detailed algorithm system for the dynamic control of container operation modes (frozen, chilled, and defrosting modes). This would allow users to measure the energy consumed throughout their operation in transit more accurately (Shinoda et al., 2022). Also, pallet stacks' fruit and packaging boxes can be explicitly modelled to characterise airflow and cooling patterns in an RC. Explicit modelling would drastically reduce the prediction error caused by the porous media assumption, but may still be outside what is currently computationally possible. Additional factors to be explored are more realistic geometrical models of refrigeration units. These refrigeration unit models would need to be validated experimentally (cooling and airflow) to ensure the airflow is delivered into the container realistically, which may influence predictions relating to the recirculation zone. Furthermore, digital twinning approaches could be applied to couple container cooling predictions with fruit quality forecasts (Lee et al.,

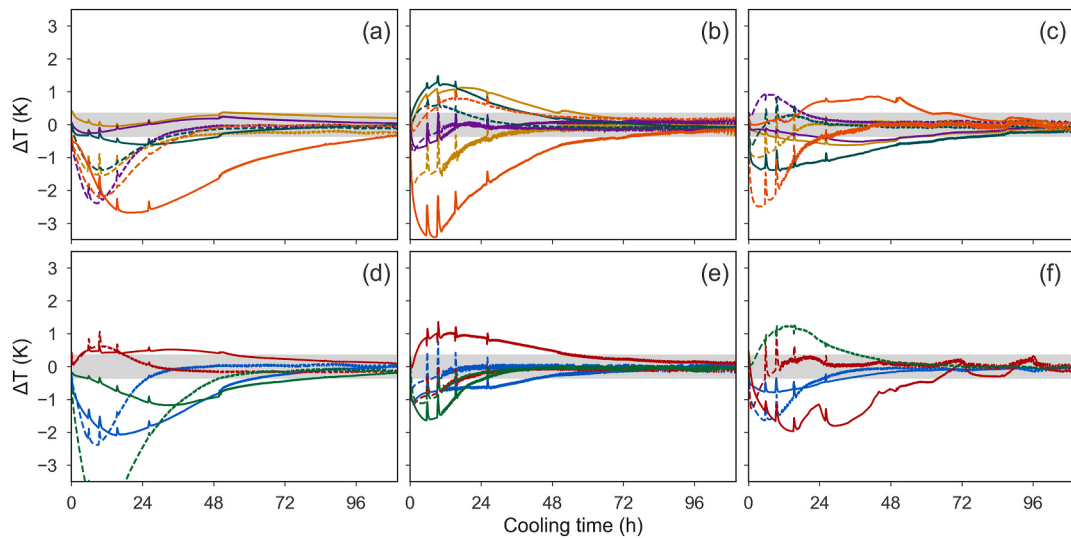


Fig. 21. Cooling-time profiles of the temperature difference ($\Delta T = T_p - T_a$) recorded by in-container loggers. Panels (a–c) represent the right-hand pallet row (R01, R03, R06, R09); panels (d–f) the left-hand row (L02, L05, L10). Columns correspond to centre, midline, and side positions. For each pallet, the top probe is plotted as a solid line and the bottom probe as a dashed line; colours identify pallets (L02 blue, L05 red, L10 green, R01 amber, R03 purple, R06 teal, R09 orange). The grey band shows the logger accuracy of ± 0.35 °C. The top-side air sensor of L10 was inactive, so no corresponding trace is shown. (For interpretation of the references to colour in this figure legend, the reader is referred to the Web version of this article.)

2022; Shrivastava et al., 2022).

5. Conclusions

This study developed and validated a CFD model to characterise airflow and heat transfer inside a refrigerated container with a dynamic refrigeration unit. The simulations and measurements together showed that airflow inside a loaded container was mainly vertical and was governed by the balance between the overall geometry inside the container and the packaging ventilation specifications (pallet airflow resistance properties). A detailed analysis of the airflow distribution within the container highlighted several unique airflow zones, one of which includes an undesirable recirculation region near the refrigeration unit. Once the cooling process in the container stabilised, air loggers placed inside cartons and between the fruit recorded temperatures consistent with fruit-pulp values. This confirms that, when sensors are correctly positioned, air temperature can serve as a reliable proxy for pulp temperature.

Finally, the study used the experimental and simulated results to propose an optimal monitoring position (ϕ position) for commercial operations limited to a single monitoring device. This position effectively monitors the cool-down process and the stabilisation of warm spots during shipping. The finding provided valuable guidance to enhance temperature monitoring practices, ensuring the quality and safety of produce. The insights gained can improve RC operation, reduce waste, and enhance sustainability in the fresh produce supply chain.

CRediT authorship contribution statement

Tarl M. Berry: Writing – review & editing, Writing – original draft, Visualization, Validation, Supervision, Project administration, Methodology, Investigation, Funding acquisition, Formal analysis, Data curation, Conceptualization. **Nurayn A. Tiamiyu:** Writing – original draft, Visualization, Validation, Formal analysis. **Jacques van Zyl:** Writing – original draft, Visualization, Validation, Methodology, Formal analysis. **Umezuruike L. Opara:** Writing – review & editing, Supervision, Conceptualization. **Paul Cronje:** Writing – review & editing, Methodology, Funding acquisition. **Alemayehu Ambaw:** Writing – review & editing, Supervision. **Vaughan Hattingh:** Writing – review & editing, Funding acquisition, Conceptualization. **Corné Coetzee:** Writing – review & editing, Supervision, Methodology, Investigation. **Thijs Defraeye:** Writing – review & editing, Writing – original draft, Methodology, Formal analysis.

Science4Impact statement

This study addresses the challenge of temperature heterogeneity and chilling injury in refrigerated containers, essential for transporting fresh produce to international markets. The study first developed and validated a computational fluid dynamics model to characterise airflow and heat transfer in a refrigerated container loaded with citrus. Key airflow and temperature regions were identified and an improved monitoring location was proposed. Additionally, an approach to monitor fruit pulp temperatures using air temperature data was detailed. These findings have already been adopted by some South African industry stakeholders, providing practical solutions for monitoring and interpreting temperature data from container shipments. This enables stakeholders to mitigate chilling injury risks and enhance the sustainability of the cold chain. Internationally, the proposed position-selection approach offers a clear route to developing policies that harmonise temperature monitoring standards, towards lower instrumentation costs and more transparent audits of cold-chain performance.

Data availability

These datasets are available from the corresponding author (T.M.

Berry) upon reasonable request for non-commercial research purposes.

Declaration of competing interest

The authors declare that they have no known competing financial interests or personal relationships that could have appeared to influence the work reported in this paper.

Acknowledgements

We gratefully acknowledge the financial support from Citrus Research International. Computations were performed using the University of Stellenbosch HPC1 (Rhasatsha): <http://www.sun.ac.za/hpc>. This work was further supported by the South African Research Chairs Initiative of the Department of Science and Technology and the National Research Foundation. We would also like to acknowledge the critical support and assistance of Sundays River Citrus Company during our experimental trials.

Appendix A. Supplementary data

Supplementary data to this article can be found online at <https://doi.org/10.1016/j.biosystemseng.2025.104254>.

References

- Ajani, C. K., Zhu, Z., & Sun, D.-W. (2021). Recent advances in multiscale CFD modelling of cooling processes and systems for the agrifood industry. *Critical Reviews in Food Science and Nutrition*, 61, 2455–2470. <https://doi.org/10.1080/10408398.2020.1809992>
- Berry, T. M., Defraeye, T., Ambaw, A., Coetzee, C. J., & Opara, U. L. (2022a). Exploring novel carton footprints for improved refrigerated-container usage and a more efficient supply chain. *Biosystems Engineering*, 220, 181–202. <https://doi.org/10.1016/j.biosystemseng.2022.06.001>
- Berry, T. M., Defraeye, T., Nicolai, B. M., & Opara, U. L. (2016). Multiparameter analysis of cooling efficiency of ventilated fruit cartons using CFD: Impact of vent-hole design and internal packaging. *Food and Bioprocess Technology*, 9, 1481–1493. <https://doi.org/10.1007/s11947-016-1733-y>
- Berry, T. M., Defraeye, T., Wu, W., Sibya, M. G., North, J., & Cronjé, P. J. R. (2021). Cooling of ambient-loaded citrus in refrigerated containers: What impacts do packaging and loading temperature have? *Biosystems Engineering*, 201, 11–22. <https://doi.org/10.1016/j.biosystemseng.2020.11.002>
- Berry, T. M., Shrivastava, C., Ambaw, A., Coetzee, C. J., Opara, U. L., & Defraeye, T. (2022). Designing ventilated packaging for the fresh-produce cold chain. *Food and Bioproducts Processing*, 134, 121–149. <https://doi.org/10.1016/j.fbp.2022.04.005>
- Cronje, P. J. R., Barry, G. H., & Huysamer, M. (2011). Postharvest rind breakdown of ‘Nules Clementine’ mandarin is influenced by ethylene application, storage temperature and storage duration. *Postharvest Biology and Technology*, 60, 192–201. <https://doi.org/10.1016/j.postharvbio.2011.01.009>
- Defraeye, T., Lambrecht, R., Ambaw, A., Delele, M. A., Opara, U. L., Cronjé, P. J. R., Verboven, P., & Nicolai, B. M. (2013). Forced-convective cooling of citrus fruit: Package design. *Journal of Food Engineering*, 118, 8–18. <https://doi.org/10.1016/j.jfoodeng.2013.03.026>
- Defraeye, T., Lukasse, L., Shrivastava, C., Verreydt, C., Schemminger, J., Cronjé, P., & Berry, T. (2022). Is there a systematic hidden ‘hot spot’ in refrigerated containers filled with fresh food in ventilated packaging? *Trends in Food Science & Technology*, 129, 388–396. <https://doi.org/10.1016/j.tifs.2022.09.005>
- Defraeye, T., Nicolai, B. M., Kirkman, W., Moore, S. D., Van Niekerk, S., Pieters, P., Cronjé, P. J. R., & Verboven, P. (2016). Integral performance evaluation of the fresh-produce cold chain: A case study for ambient loading of citrus in refrigerated containers. *Postharvest Biology and Technology*, 112, 1–13. <https://doi.org/10.1016/j.postharvbio.2015.09.033>
- Defraeye, T., Verreydt, C., Gonthier, J., Lukasse, L. L., Cronje, P., & Berry, T. M. (2023). Building a physics-based virtual refrigerated container filled with fruit in ventilated packaging. *MethodsX*, 13, Article 102984. <https://doi.org/10.1016/j.mex.2024.102984>
- Defraeye, T., Verreydt, C., Gonthier, J., Lukasse, L. L., Cronje, P., & Berry, T. M. (2024). The virtual container: Physics-based simulation of refrigerated container map temperature and fruit quality evolution and variability in a shipment. *Postharvest Biology and Technology*, 211, Article 112722. <https://doi.org/10.1016/j.postharvbio.2023.112722>
- Fadiji, T. S., Coetzee, C. J., & Opara, U. L. (2016). Compression strength of ventilated corrugated paperboard packages: Numerical modelling, experimental validation and effects of vent geometric design. *Biosystems Engineering*, 151, 231–247. <https://doi.org/10.1016/j.biosystemseng.2016.09.010>
- Fitzgerald, W. B., Howitt, O. J. A., Smith, I. J., & Hume, A. (2011). Energy use of integral refrigerated containers in maritime transportation. *Energy Policy*, 39, 1885–1896. <https://doi.org/10.1016/j.enpol.2010.12.015>

- Food and Agriculture Organization (FAO). (2018). *Ispm 42: Requirements for the use of temperature treatments as phytosanitary measures*. Rome, Italy: International plant protection convention. Food and Agriculture Organization.
- Food and Agriculture Organization (FAO). (2021). *World food and agriculture: Statistical yearbook 2021*. FAO. <https://www.fao.org/3/cb4477en/cb4477en.pdf>.
- Gesamtverband der Deutschen Versicherungswirtschaft e.V. (GDV). (2012). Air flow and regulation (section 8.4.2.1). In *Container handbook* (Vol. 3) Berlin, Germany: Gesamtverband der Deutschen Versicherungswirtschaft e.V.
- Getahun, S., Ambaw, A., Delele, M. A., Meyer, C. J., & Opara, U. L. (2017a). Analysis of airflow and heat transfer inside fruit-packed refrigerated shipping container: Part I – Model development and validation. *Journal of Food Engineering*, 203, 58–68. <https://doi.org/10.1016/j.jfoodeng.2017.02.010>
- Getahun, S., Ambaw, A., Delele, M. A., Meyer, C. J., & Opara, U. L. (2017b). Analysis of airflow and heat transfer inside fruit-packed refrigerated shipping container: Part II – Evaluation of apple packaging design and vertical flow resistance. *Journal of Food Engineering*, 203, 83–94. <https://doi.org/10.1016/j.jfoodeng.2017.02.011>
- Heyes, J. (2023). Impact of chilling injury on global trade in tropical products. *CABI Reviews*, 18. <https://doi.org/10.1079/cabireviews.2023.0037>. Article 0037.
- Hoang, H.-M., Duret, S., Flick, D., & Laguerre, O. (2015). Preliminary study of airflow and heat transfer in a cold room filled with apple pallets: Comparison between two modelling approaches and experimental results. *Applied Thermal Engineering*, 76, 367–381. <https://doi.org/10.1016/j.applthermaleng.2014.11.012>
- International Organization for Standardization (ISO). (2018). *Series 1 freight containers — Specification and testing — Part 2: Thermal containers*. Geneva: ISO. ISO Standard No. 1496-2:2018.
- International Organization for Standardization (ISO). (2020). *Series 1 freight containers — Classification, dimensions and ratings*. In *ISO 668:2020*. Geneva: ISO.
- Issa, S., & Lang, W. (2016). Airflow simulation inside reefer containers. In H. Kotzab, J. Pannek, & K. D. Thoben (Eds.), *Proceedings of the 4th international conference LDIC, 2014, Bremen, Germany* (pp. 303–311). Cham, Switzerland: Springer. https://doi.org/10.1007/978-3-319-23512-7_29.
- Jedermann, R., Geyer, M., Praeger, U., & Lang, W. (2013). Sea transport of bananas in containers: Parameter identification for a temperature model. *Journal of Food Engineering*, 115, 330–338. <https://doi.org/10.1016/j.jfoodeng.2012.10.039>
- Jiang, T., Xu, N., Luo, B., Deng, L., Wang, S., Gao, Q., & Zhang, Y. (2020). Analysis of an internal structure for refrigerated container: Improving distribution of cooling capacity. *International Journal of Refrigeration*, 113, 228–238. <https://doi.org/10.1016/j.ijrefrig.2020.01.023>
- Kader, A. A. (2002). *Postharvest technology of horticultural crops* (3rd ed.). Davis, CA: University of California Agriculture and Natural Resources.
- Laguerre, O., Ben Amara, S., Alvarez, G., & Flick, D. (2008). Transient heat transfer by free convection in a packed bed of spheres: Comparison between two modelling approaches and experimental results. *Applied Thermal Engineering*, 28, 14–24. <https://doi.org/10.1016/j.applthermaleng.2007.03.014>
- Lee, H., Park, S., Lee, S., Lee, S., & Lee, K. (2022). Development of a machine-learning model for reefer-container failure determination and cause analysis with unbalanced data. *Journal of the Korea Convergence Society*, 13, 23–30. <https://doi.org/10.15207/JKCS.2022.13.01.023>
- Lukasse, L. J. S., Baerentz, M. B., & Kramer-Cuppen, J. E. D. (2011). Quest II: Reduction of CO₂ emissions of reefer containers. In *Proceedings of the 23rd IIR international congress of refrigeration* (pp. 3203–3210). Montréal, Canada: International Institute of Refrigeration.
- Lukasse, L. J. S., Schouten, R. E., Castelein, R. B., Lawton, R., Paillart, M. J. M., Guo, X., Woltering, E. J., Tromp, S., Snels, J. C. M. A., & Defraeye, T. (2023). Perspectives on the evolution of reefer containers for transporting fresh produce. *Trends in Food Science & Technology*, 140, Article 104147. <https://doi.org/10.1016/j.tifs.2023.104147>
- Lukasse, L. J. S., & Snels, J. J. (2022). *Estimating temperatures in refrigerated containers and trailers (Wageningen food & biobased research report 2233)*. Wageningen, Netherlands: Wageningen University & Research. <https://edepot.wur.nl/569574>.
- Maiorino, A., Petruzzello, F., & Aprea, C. (2021). Refrigerated transport: State of the art, technical issues, innovations and challenges for sustainability. *Energies*, 14, 7237. <https://doi.org/10.3390/en14217237>
- Moore, S. D., & Hattingh, V. (2016). *A review of control measures and risk-mitigation options for false codling moth (*Thaumatomibia leucotreta*) and their efficacy* (technical report). Citrus Research International. <https://www.citrusres.com/wp-content/uploads/2021/08/FCM-risk-mitigation-and-control-review-Dec-2016.pdf>.
- Moore, S. D., Kirkman, W., Albertyn, S., Love, C. N., Coetzee, J. A., & Hattingh, V. (2016). Partial cold treatment of citrus fruit for export risk mitigation for *Thaumatomibia leucotreta* (Lepidoptera: Tortricidae) as part of a systems approach. *Journal of Economic Entomology*, 109, 1578–1585. <https://doi.org/10.1093/jee/tow138>
- Moureh, J., Menia, N., & Flick, D. (2002). Numerical and experimental study of airflow in a typical refrigerated truck configuration loaded with pallets. *Computers and Electronics in Agriculture*, 34, 25–42. [https://doi.org/10.1016/S0168-1699\(01\)00178-8](https://doi.org/10.1016/S0168-1699(01)00178-8)
- Moureh, J., Tapsoba, S., Derens, E., & Flick, D. (2009). Air-velocity characteristics within vented pallets loaded in a refrigerated vehicle with and without air ducts. *International Journal of Refrigeration*, 32, 220–234. <https://doi.org/10.1016/j.ijrefrig.2008.06.006>
- Mukama, M., Ambaw, A., & Opara, U. L. (2020). Advances in design and performance evaluation of fresh-fruit ventilated distribution packaging: A review. *Food Packaging and Shelf Life*, 24, Article 100472. <https://doi.org/10.1016/j.fpsl.2020.100472>
- Norton, T., & Sun, D.-W. (2006). Computational fluid dynamics—an effective and efficient design and analysis tool for the food industry: A review. *Trends in Food Science & Technology*, 17, 600–620. <https://doi.org/10.1016/j.tifs.2006.05.004>
- O'Sullivan, J. L., Ferrua, M. J., Love, R. J., Verboven, P., Nicolai, B. M., & East, A. R. (2017). Forced-air cooling of polyblended horticultural produce: Optimal cooling conditions and package design. *Postharvest Biology and Technology*, 126, 67–75. <https://doi.org/10.1016/j.postharbio.2016.11.019>
- Rhodes, M. (2008). Fluid flow through a packed bed of particles. In *Introduction to particle technology* (2nd ed., pp. 153–168). Hoboken, NJ: Wiley.
- Robertson, G. L. (2013). *Food packaging: Principles and practice* (3rd ed.). Boca Raton, FL: CRC Press.
- Scharnow, R. (2014). Maintaining the quality of highly perishable goods. In U. Duken, K. Handrack, G. Naber, & U.-P. Schieder (Eds.), *Container handbook*. Berlin, Germany: Marine and Loss Prevention Department of Gesamtverband der Deutschen Versicherungswirtschaft.
- Senguttuvan, S., Rhee, Y., Lee, J., Kim, J., & Kim, S. M. (2021). Enhanced heat transfer in a refrigerated container using an airflow-optimised refrigeration unit. *International Journal of Refrigeration*, 131, 723–736. <https://doi.org/10.1016/j.ijrefrig.2021.02.017>
- Senguttuvan, S., Youn, J. S., Park, J., Lee, J., & Kim, S. M. (2020). Enhanced airflow in a refrigerated container by improving the refrigeration-unit design. *International Journal of Refrigeration*, 120, 460–473. <https://doi.org/10.1016/j.ijrefrig.2020.08.019>
- Shinoda, T., Budiyanto, M. A., & Sugimura, Y. (2022). Analysis of energy conservation by roof-shade installations in refrigerated-containers areas. *Journal of Cleaner Production*, 377, Article 134402. <https://doi.org/10.1016/j.jclepro.2022.134402>
- Shrivastava, C., Berry, T., Cronje, P., Schudel, S., & Defraeye, T. (2022). Digital twins enable the quantification of trade-offs in maintaining citrus quality and marketability in the refrigerated supply chain. *Nature Food*, 3, 413–427. <https://doi.org/10.1038/s43016-022-00497-9>
- Smale, N. J. (2004). *Mathematical modelling of airflow in shipping systems: Model development and testing*. Palmerston North, New Zealand: Massey Research Online. Doctoral dissertation, Massey University <http://hdl.handle.net/10179/1718>.
- Tanner, D. J., & Amos, N. D. (2003). Temperature variability during shipment of fresh produce. *Acta Horticulturae*, 599, 193–203. <https://doi.org/10.17660/ActaHortic.2003.599.24>
- Thompson, J. F. (2004). Pre-cooling and storage facilities. In K. Gross, & J. F. Thompson (Eds.), *The commercial storage of fruits, vegetables, and florist and nursery stocks (Agriculture Handbook No. 66)*. Washington, DC: U.S. Department of Agriculture.
- Thompson, J. F., Mejia, D. C., & Singh, R. P. (2010). Energy use of commercial forced-air coolers for fruit. *Applied Engineering in Agriculture*, 26, 919–924.
- Thompson, J. F., Mitchell, F. G., Rumsey, T. R., Kasmiye, R. F., & Crisosto, C. H. (2008). *Commercial cooling of fruits, vegetables, and flowers (publication 21567)*. Oakland, CA: University of California Agriculture and Natural Resources.
- Tiamiyu, N. A. (2020). *Exploring next-generation packaging systems in a refrigerated container using CFD modelling* (Master's thesis, stellendbosch university, stellendbosch, South Africa). SUNScholar Research Repository. <https://hdl.handle.net/10019.1/109368>.
- Verboven, P., Flick, D., Nicolai, B. M., & Alvarez, G. (2006). Modelling transport phenomena in refrigerated food bulks, packages and stacks: Basics and advances. *International Journal of Refrigeration*, 29, 985–997. <https://doi.org/10.1016/j.ijrefrig.2005.12.010>
- Vines, H. M., Edwards, G. J., & Grierson, W. (1965). Citrus-fruit respiration. *Proceedings of the Florida State Horticultural Society*, 78, 198–201.
- Wild, Y. (2014). Technical aspects during transportation. In U. Duken, K. Handrack, G. Naber, & U.-P. Schieder (Eds.), *Container handbook*. Berlin, Germany: Marine and Loss Prevention Department of Gesamtverband der Deutschen Versicherungswirtschaft.
- Wu, W., Cronje, P. J. R., Verboven, P., & Defraeye, T. (2019). Unveiling how ventilated-packaging design and cold-chain scenarios affect the cooling kinetics and fruit quality for each single citrus fruit in an entire pallet. *Food Packaging and Shelf Life*, 21, Article 100369. <https://doi.org/10.1016/j.fpsl.2019.100369>
- Zacarias, L., Cronje, P., & Palou, L. (2020). Postharvest technology of citrus fruits. In M. Talon, M. Caruso, & F. Gmitter (Eds.), *The genus citrus* (pp. 421–446). Cambridge, UK: Woodhead Publishing.
- Zhao, C.-J., Han, J.-W., Yang, X.-T., Qian, J. P., & Fan, B.-L. (2016). A review of computational fluid dynamics for the forced-air cooling process. *Applied Energy*, 168, 314–331. <https://doi.org/10.1016/j.apenergy.2016.01.101>